ARMY RESEARCH LABORATORY

Evaluation of the Weather Research and Forecast Model Over Dugway, Utah, During 2009

by Jeffrey Passner, Robert Dumais, Barbara Sauter, and Robert Flanigan

ARL-TR-5032 **November 2009**

NOTICES

Disclaimers

The findings in this report are not to be construed as an official Department of the Army position unless so designated by other authorized documents.

Citation of manufacturer's or trade names does not constitute an official endorsement or approval of the use thereof.

Destroy this report when it is no longer needed. Do not return it to the originator.

Army Research Laboratory
White Sands Missile Range, NM 88002-5513

ARL-TR-5032 **November 2009**

Evaluation of the Weather Research and Forecast Model Over Dugway, Utah, During 2009

Jeffrey Passner, Robert Dumais, Barbara Sauter, and Robert Flanigan
Computational and Information Sciences Directorate, ARL

REPORT DOCUMENTATION PAGE	Form Approved OMB No. 0704-0188

1. REPORT DATE *(DD-MM-YYYY)*	2. REPORT TYPE	3. DATES COVERED (From - To)
November 2009	Final	October 2008–October 2009

4. TITLE AND SUBTITLE
Evaluation of the Weather Research and Forecast Model Over Dugway, Utah, During 2009

5a. CONTRACT NUMBER

5b. GRANT NUMBER

5c. PROGRAM ELEMENT NUMBER

6. AUTHOR(S)
Jeffrey Passner, Robert Dumais, Barbara Sauter, and Robert Flanigan

5d. PROJECT NUMBER

5e. TASK NUMBER

5f. WORK UNIT NUMBER

7. PERFORMING ORGANIZATION NAME(S) AND ADDRESS(ES)
U.S. Army Research Laboratory
Computational and Information Sciences Directorate
Battlefield Environment Division (ATTN: RDRL-CIE-M)
White Sands Missile Range, NM 88002-5501

8. PERFORMING ORGANIZATION REPORT NUMBER
ARL-TR-5032

9. SPONSORING/MONITORING AGENCY NAME(S) AND ADDRESS(ES)

10. SPONSOR/MONITOR'S ACRONYM(S)

11. SPONSOR/MONITOR'S REPORT NUMBER(S)

12. DISTRIBUTION/AVAILABILITY STATEMENT
Approved for public release; distribution is unlimited.

13. SUPPLEMENTARY NOTES

14. ABSTRACT
The U.S. Army Research Laboratory (ARL) performed numerous case studies of the Advanced Research version of the Weather Research and Forecasting (WRF) model at horizontal resolutions of 3 and 1 km to better understand weather output for military use. ARL's devised model sensitivity experiments of several WRF parameterizations including the vertical resolution of 40, 60, and 80 levels, model time steps of 9 and 3 seconds, three different explicit microphysics, and the two planetary boundary layer options. Model output was studied for numerous different meteorological parameters, but most of the effort was aimed at analyzing surface features such as wind, temperature, moisture, and precipitation to better understand how the different parameterizations influenced the surface-based observations. Four diverse meteorological days were studied and statistical results showed little difference between each model simulation. However, significant differences in some of the meteorological variables and some model errors were discovered. These model discrepancies are discussed in detail.

15. SUBJECT TERMS
WRF, mesoscale, resolution, statistics, wind, model

16. SECURITY CLASSIFICATION OF:			17. LIMITATION OF ABSTRACT	18. NUMBER OF PAGES	19a. NAME OF RESPONSIBLE PERSON
a. REPORT	b. ABSTRACT	c. THIS PAGE			Jeffrey Passner
Unclassified	Unclassified	Unclassified	UU	68	19b. TELEPHONE NUMBER (*Include area code*) (575) 678-8547

Standard Form 298 (Rev. 8/98)
Prescribed by ANSI Std. Z39.18

Contents

List of Figures

List of Tables

Acknowledgments

The error statistics included in this data report were generated using the Model Evaluation Tools (MET), developed at the National Center for Atmospheric Research (NCAR) through a grant from the United States Air Force Weather Agency (AFWA). NCAR is sponsored by the United States National Science Foundation.

In addition, AFWA provided funding and guidance to the U.S. Army Research Laboratory (ARL) to provide Numerical Weather Prediction (NWP) model research.

1. Summary

The U.S. Army Research Laboratory (ARL) conducted numerous model runs of the Advanced Research version of the Weather Research and Forecasting (WRF) model at horizontal resolutions of 3 and 1 km. ARL's research emphasis in this study focused on sensitivity experiments of the model parameterizations including model time steps, vertical resolution, explicit microphysics, and the planetary boundary layer. Model output was studied for numerous different meteorological parameters but most of the effort was aimed at analyzing surface features such as wind, temperature, moisture, and precipitation to better understand how the different parameterizations influenced the surface-based observations.

2. Introduction

The U.S. Army Research Laboratory (ARL) Battlefield Environment Directorate (BED) has performed research involving various aspects of the Advanced Research version of the Weather Research and Forecasting (WRF-ARW) model (Skamarock et al., 2008) version 3.0.1.1 during 2009. This research focuses primarily on the utility of the WRF-ARW for limited-area short-range forecast and nowcast purposes at grid spacing ranging between 0.3 km and 3 km, and is being partially supported through the Air Force Weather Agency (AFWA). ARL tested various perturbations involving model vertical resolution, time stepping, microphysics, planetary boundary layer (PBL) and turbulence parameterization, observation nudging data assimilation, and sub-nesting to hundreds of meters grid spacing (Dumais et al., 2009). To provide proper metrics using traditional statistical and newer object- based verification approaches, the National Center for Atmospheric Research (NCAR) Model Evaluation Tool (MET) was implemented as a part of this research (see Model Evaluation Tools | DTC User's Support Page in the references).

ARL has performed case studies investigating the performance of various Numerical Weather Prediction (NWP) models over many years to highlight appropriate weather forecast applications for predominantly military use. Previous studies have included some traditional statistical measures including mean error (ME), mean absolute error (MAE), and root mean square error (RMSE) values, but resource constraints dictated a fairly small number of data points used for the calculations. The development of MET allows for more comprehensive statistical evaluations of current DoD options for using the Weather Research and Forecasting (WRF) model. MET was used to generate ME, MAE, and RMSE values based on weekly WRF runs over a 10-week period during the spring months of 2009. As a matter of convenience, results are noted to two decimal places even though the data are not significant to that degree of accuracy.

Wind direction errors were omitted for any observed wind speed less than 1 m/s.* MET calculates wind direction mean errors in two different ways.

1. For the "ROW_MEAN_WDIR" line, each of the input lines are treated separately and given equal weight. The mean forecast wind direction, mean observation wind direction, and the associated error are computed for each of these lines. Then the means are computed across all of these forecast wind directions, observation wind directions, and their errors.

2. For the "AGGR_WDIR" line, the input lines are first aggregated into a single line of partial sums where the weight for each line is determined by the number of points it represents. From this aggregated line, the mean forecast wind direction, observation wind direction, and the associated error are computed and written out.

Both are included in this report, although the errors seem smaller than expected. Bias values near 180 degrees are misleading since they are actually very close to a 0 degree bias.

A second research area is focused upon the development of the WRF-ARW four-dimensional data assimilation (FDDA) for the same limited area domains and grid space resolutions being studied over the Dugway Proving Ground (DPG), UT, region. The model version used in this part of the study was WRF version 3.1. A final research effort is investigating the potential for sub-kilometer grid space nesting in the WRF-ARW, and is aimed at exploring issues such as whether or not to use PBL parameterization, terrain treatment, lateral boundary condition effects, two-way nesting potential, domain size and computational feasibility, and time step influence. Neither of these two research areas will be discussed in this report.

3. Model Configuration

The model runs in this study use a 3-km and 1-km double nest configuration, and the National Center of Environmental Prediction's WRF-based North American Model (NAM) 218 grids as initial conditions and lateral boundary conditions for the outer nest. The specifications of the ARL WRF-ARW nests, along with a control set of namelist (model control) options, are shown in table 1.

* Note that "s" or "sec" is used interchangeable throughout this report for the unit "second."

Table 1. Namelist options for WRF-ARW control run used in this model study.

Namelist Parameter	Option Selected
Shortwave radiation scheme	Dudhia scheme
Longwave radiation scheme	RRTM
Explicit moist microphysics	WSM-5 class
Cumulus parameterization	None on both nests
PBL scheme	Yonsei State University (YSU) non-local closure
Surface layer	Monin-Obukhov
Land surface scheme	NOAH land-surface model
Time step (sec) to grid-spacing (km) ratio	3:1
Horizontal subgrid diffusion	2nd order on coordinate surfaces
Subgrid turbulence closure	Horizontal Smagorinsky 1st order closure
Number of vertical etap (eta-pressure) terrain-following levels	60
Vertical velocity damping	Yes
Feedback	Yes–with smooth-desmooth-smooth filter
Nesting	Two-way
Terrain slope/shadow	Yes

In table 2, the set of perturbations from the control run that are also being simulated are shown.

Table 2. Individual simulation perturbations from WRF-ARW control run that were executed.

Thompson explicit moist microphysics
Lin explicit microphysics
Mellow-Yamada-Janic (MYJ) PBL scheme with MYJ surface layer
Time steps (s) to grid spacing (km) ratio of 1:1
Number of vertical etap terrain-following levels =40
Number of vertical etap terrain-following levels=80

Both the control and the subset of perturbations were run for a small number of predetermined case studies, with the grid domain centered over DPG. For all cases, a full 24-hour (h) simulation period was examined starting at 0600 universal time coordinates (UTC). The location of the model domain was selected based on several factors: excellent complex terrain area with a nearby large inland lake, seasonal changes in meteorology, which run a wide spectrum of synoptic phenomena, proximity to the Utah Mesowest, and the potential for additional ground

truth boundary layer meteorology measurements via the West Desert Test Center at DPG. The size of the modeling domains was similar to what has been utilized in ARL meteorological modeling applications for the Army, while the NAM 218 is similar to the operational resolutions run currently at AFWA at a four times daily frequency (15 km, 5 km). In this particular study the outer domain (domain 1) with a 3-km resolution was 183*183 grid points while the inner nest (domain 2) was 103*103 with a 1-km resolution.

WRF output on standard surface and pressure levels was generated with the WRF Post Processor Version 3 (WPPV3), and those values were compared to point observations including surface, upper air, and radar wind data. All the observations were within 16 minutes before or after the model valid time on the hour. The observations for domain 1 were obtained from the National Center for Environmental Prediction's PrepBinary Universal Form for the Representation of meteorological data Prep(BUFR) files. These observations are considered acceptable for operational use. Approximately 20–25 PrepBUFR surface station observations were available each hour for domain 1, with only a sporadic single observation within the domain 2 grid (see figures 1 and 2). The PrepBUFR observations also include two upper air sounding locations and a single radar wind profiler site, Elko, NV, and Salt Lake City (SLC), UT, and VADWND on the map showing the two WRF domains. Based on the lack of PrepBUFR observations available for evaluation in domain 2, mesonet observations were obtained from the Meteorological Assimilation Data Ingest System (MADIS), which included up to 24 surface station observations within domain 2. No MADIS observations were available for 8 April 2009, so some of the PrepBUFR evaluations were skipped on that date. No upper air observations were available within domain 2 for this study. Many more surface observations could be incorporated into the domain 1 evaluations if MADIS mesonet observations were used rather than the PrepBUFR observations, but no attempt to use them or to compare their quality values was attempted for this study based on time constraints.

Figure 1. Domain 1, the larger grid with the smaller domain 2 over DPG.

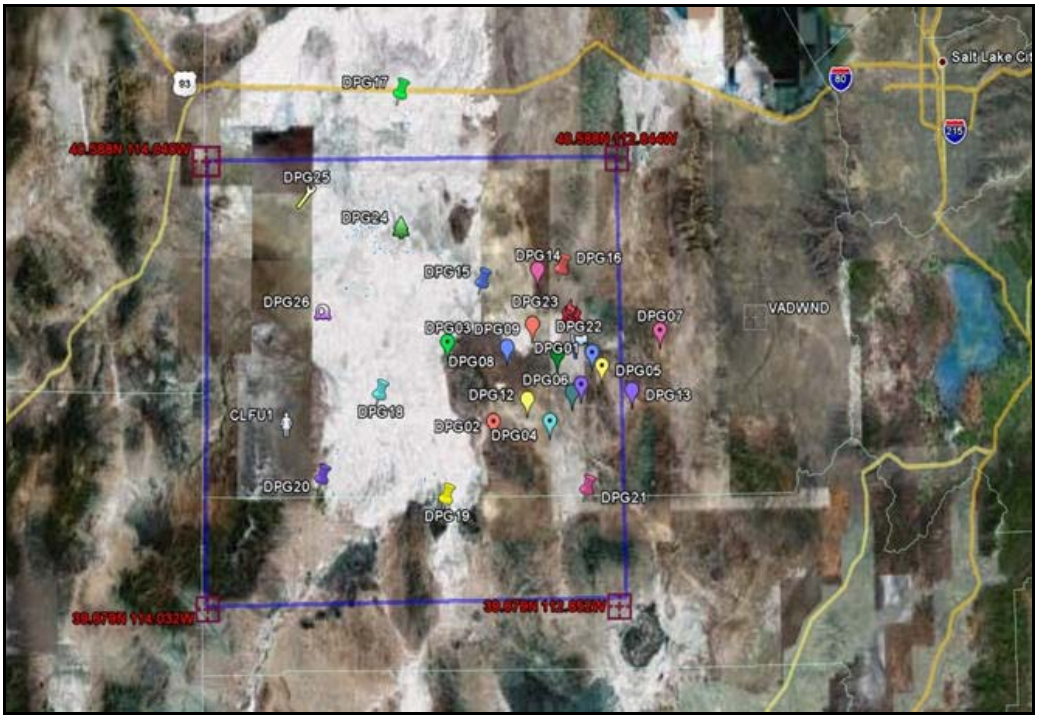

Figure 2. Domain 2, the inner nest over DPG with sites where Surface Atmospheric Measuring Systems are located.

4. Meteorological Analysis

Four model runs were done over DPG during this study, each with unique modeling issues. A description of the larger-scale weather is listed for each case.

4.1 Case 1

Case 1: 26 March 2009 – A 540 dm upper low was located just northeast of SLC at 1200 UTC, 26 March 2009 with a strong, digging jet max on the southwest side of the upper low over Nevada. At the surface, the lowest pressure was over north central Colorado with a warm front over eastern Colorado and a cold front extending from the low through southern Utah. The cold front had already passed through most of domain 1 and all of domain 2 by 0600 UTC, which led to a deep west to northwest flow at most levels of the atmosphere, along with strong northwest upslope flow on the west side of any mountain ranges. The 1200 UTC SLC sounding, as displayed in figure 3, showed a moist layer from 800 to 630 hPa with a temperature of –31.5 °C at 500 hPa, which led to considerable mid-level instability. This resulted in significant mountain snows but little snow accumulation in the valley locations due to dry air advecting in from the northwest in the boundary layer. By late afternoon, most of the region was cold and dry with winds veering to a north-northeasterly direction.

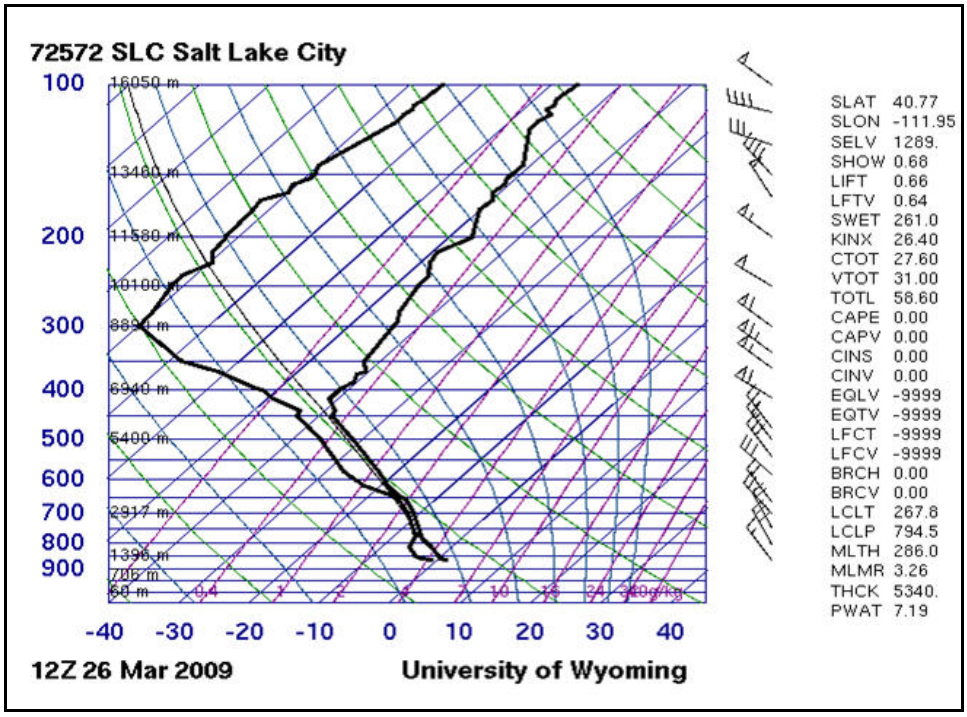

Figure 3. Upper-air observation for SLC at 1200 UTC, 26 March 2009.

Note: Source is http://weather.uwyo.edu/upperair/sounding.html.

The key focus in this model run was the precipitation amounts. As seen in the 1200 UTC SLC sounding, the layer from 650 to 800 hPa is nearly saturated. However, by 0000 UTC, 27 March 2009 (refer to figure 4), only a modest amount of moisture remains in the layer. The precipitable water has dropped from 7.19 mm to 4.10 mm at SLC and the associated mixing ratios have also diminished. Thus, as expected, much of the precipitation occurred in the early hours of the model run and over the higher terrain.

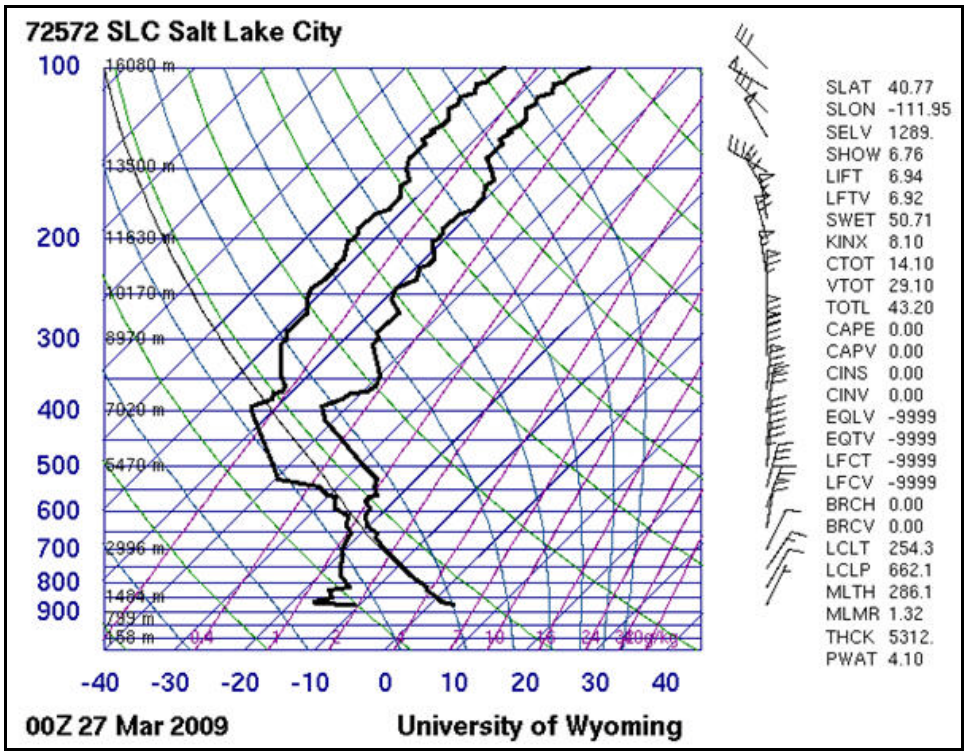

Figure 4. Upper-air observation for SLC, 27 March 2009 at 0000 UTC.

Note: Source is http://weather.uwyo.edu/upperair/sounding.html.

Since no surface observations are available on the higher terrain it becomes impossible to verify actual precipitation totals. Radar data is probably too far from the location and is not particularly useful in this case. However, there is still the issue of precipitation amount and the different parameterization over high terrain. Table 3 shows the model maximum precipitation over the high terrain of the Deep Creek Mountains on the southwestern border of domain 2.

Table 3. Total 24-h maximum precipitation (mm) from 26 March, 0600 UTC to 27 March, 0600 UTC, over Deep Creek Mountains.

Model Parameterization	24-h Total Precipitation Over Highest Peaks of The Deep Creek Mountains (mm)
Microphysics 4	50 mm
Microphysics 2	65 mm
Microphysics 8	33 mm
MYJ Boundary-layer scheme	45 mm
40 model levels	40 mm
80 model levels	50 mm
3-second time step	55 mm

Table 3 shows a wide variety in orographic precipitation with microphysics option 8 producing the lowest total (33 mm) and microphysics option 2 producing the highest total (65 mm) over the 24-h forecast period. Plotting some of the key moisture variables through the forecast does give some hints as to what the moisture differences are between microphyics 2 (Lin routine) and microphysics 8 (Thompson routine). Figure 5 shows the vertical motion field in m/sec for the Lin microphysics case while figure 6 displays the vertical motion field for Thompson's scheme.

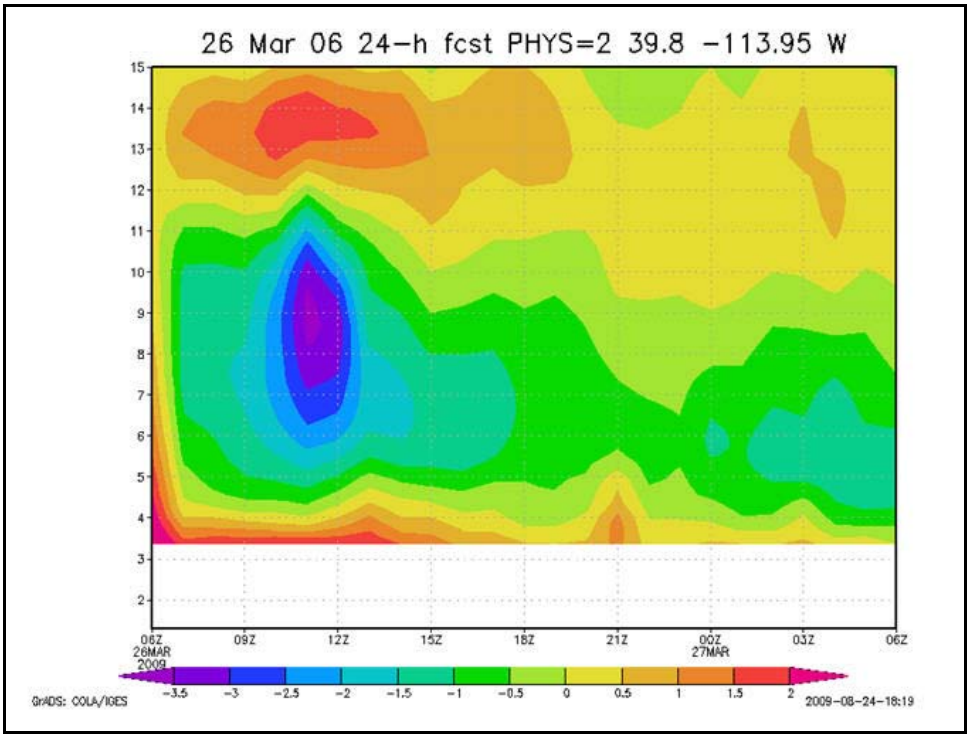

Figure 5. Vertical motion field (m/sec) from 0600 UTC, 26 March to 0600 UTC, 27 March with height (km) at 39.8N–113.95 (over Deep Creek Mountains) using microphysics 2 parameterization.

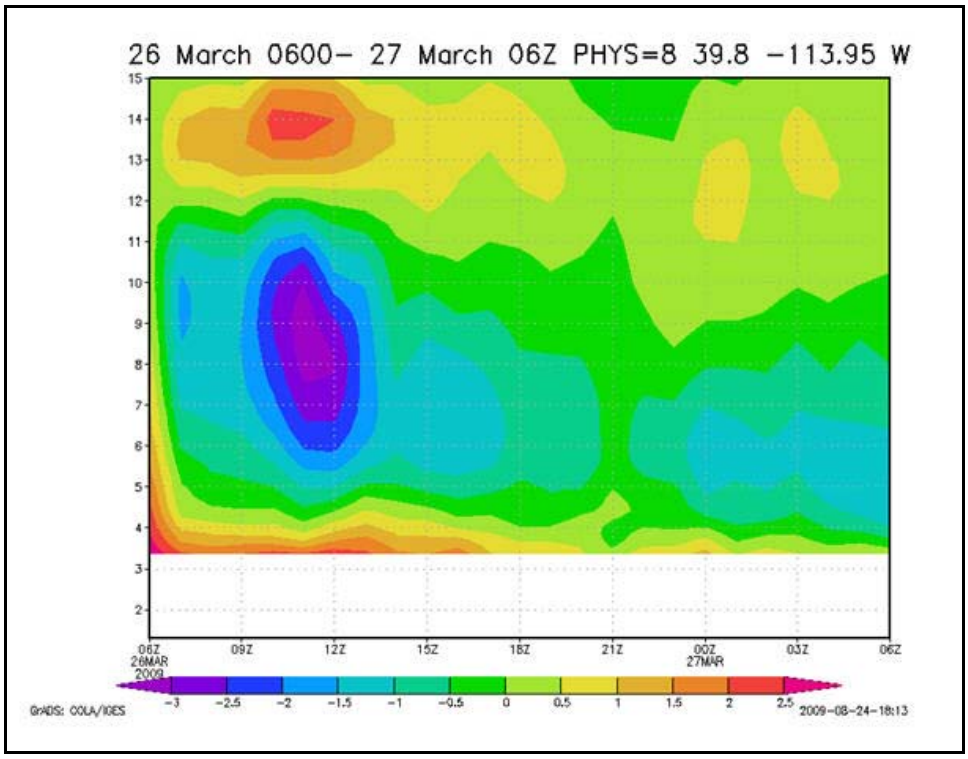

Figure 6. Vertical motion field (m/sec) from 0600 UTC, 26 March to 0600 UTC, 27 March with height (km) at 39.8N–113.95 (over Deep Creek Mountains) using microphysics 8 parameterization.

While there are minor differences in the vertical motion field, they are very similar in having a shallow layer of rising motion overlaid by a deep layer of sinking motion above it. This result was a little surprising at first because the atmosphere was unstable; however, it is possible that most of the lifting was weaker and from upslope alone on the western side of the mountain range. While not shown here, there are only slight differences in qrain (rain water mixing ratio), qsnow (snow mixing ratio), and the vertical distribution of the relative humidity (RH) in the results of the two different microphysics options. However, as figures 7 and 8 indicate, there are large discrepancies in the qice (ice mixing ratio) fields.

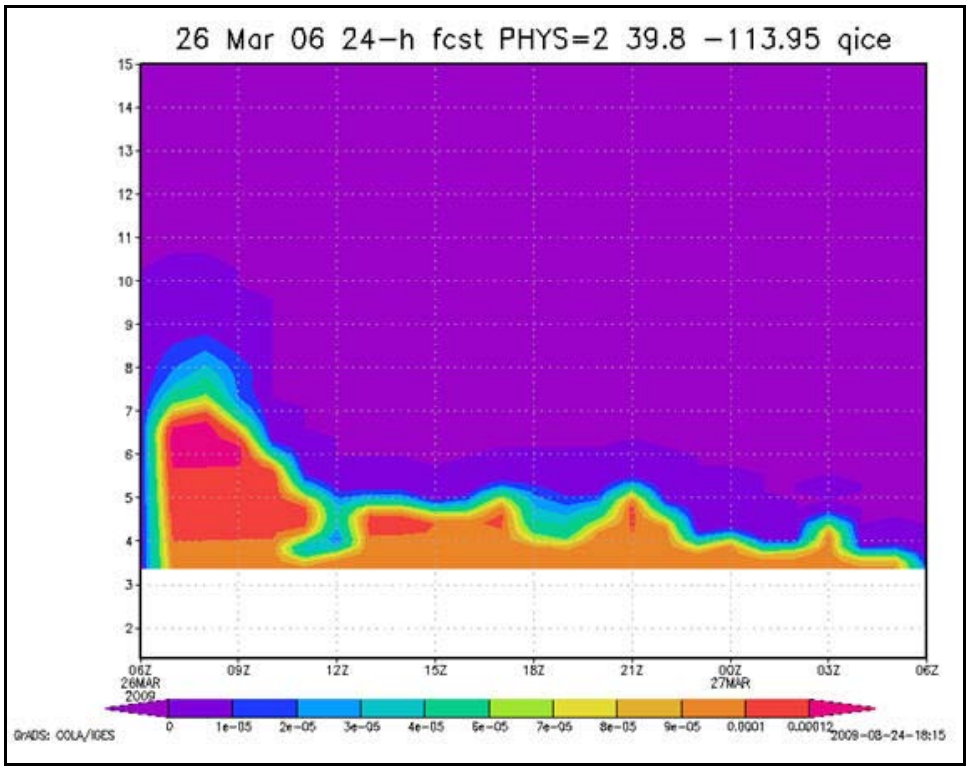

Figure 7. Qice (kg/kg) from 0600 UTC, 26 March to 0600 UTC, 27 March with height (km) at 39.8N–113.95 (over Deep Creek Mountains) using microphysics 2 parameterization.

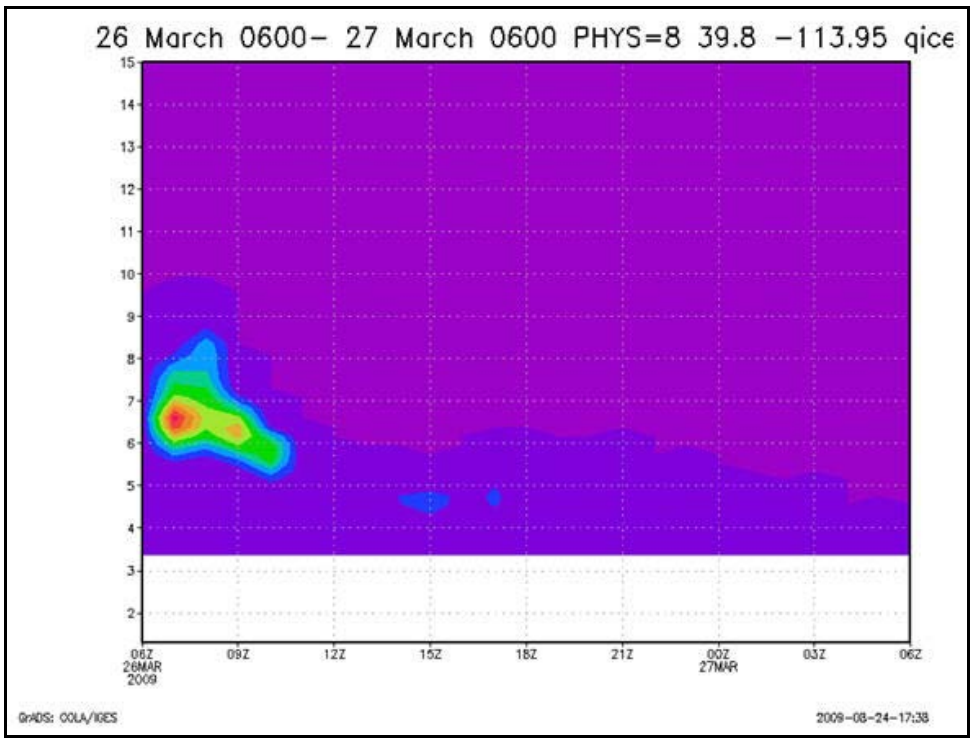

Figure 8. Qice (kg/kg) from 0600 UTC, 26 March to 0600 UTC, 27 March with height (km) at 39.8N–113.95 (over Deep Creek Mountains) using microphysics 8 parameterization.

Overall, the model performed well for this case—a highly dynamical system, with a strong surface cold front. As an example, the forecasted surface wind field at 0700 UTC, is shown in figure 9 and the observed wind field at 0700 UTC is displayed in figure 10. It can be seen that the model handled the wind directions well capturing the northwest to north surface winds over the domain. The forecasted wind speeds average about 10 m/s in the valley locations with stronger winds on the downslope or east side of the Deep Creek Mountains. Due to the lack of available observations over and near this mountain range, it is impossible to see if these wind speeds verified; however, the one observation near the mountain range does show a measured wind speed of 9 m/s.

The temperature fields were also handled well by the simulation as seen in figures 11 and 12. The forecasted temperatures were about 278 K (5 °C) in the valley area while observations were generally 4–5 °C in the region.

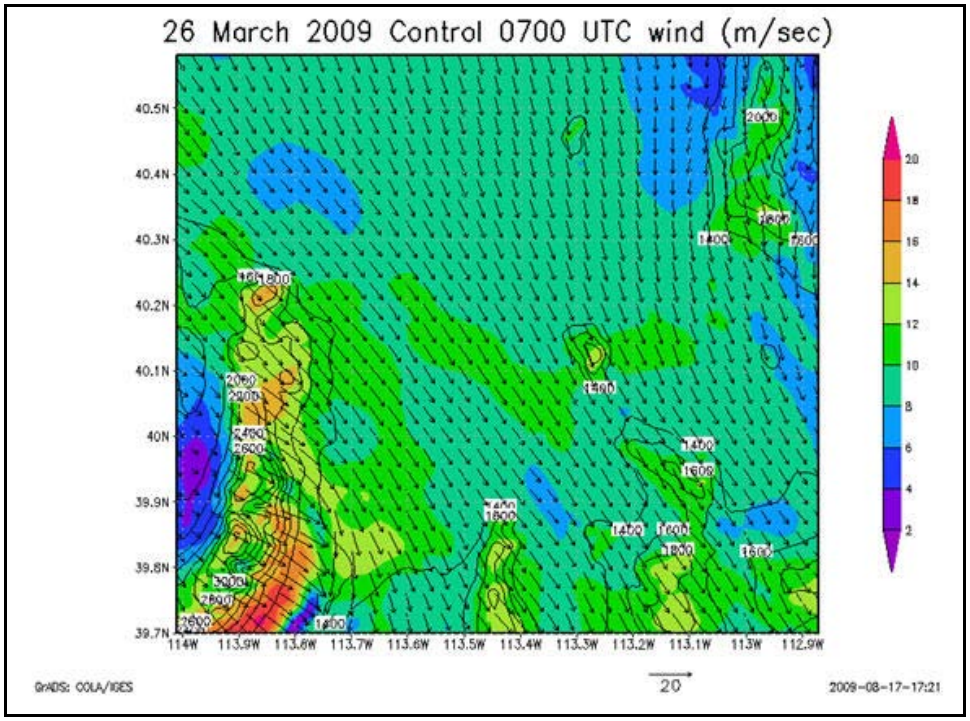

Figure 9. Wind direction (arrows) wind speed m/sec (shaded) at 0700 UTC, 26 March 2009 over domain 2 for the control run (microphysics option 4).

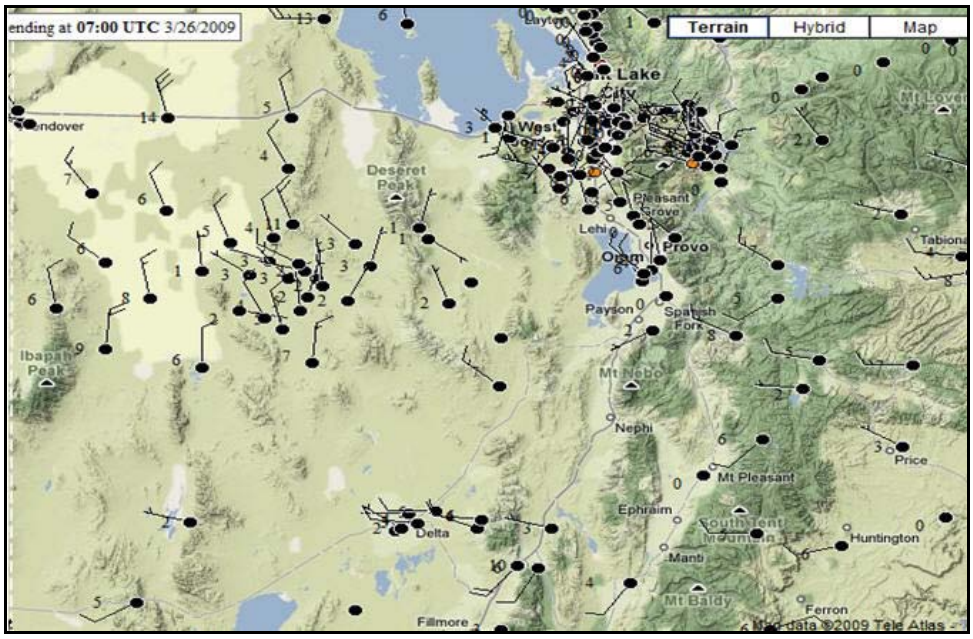

Figure 10. Wind direction (wind barbs) along with wind speed (m/s) at 0700 UTC, 26 March 2009 over domain 2 from observations on Mesowest.

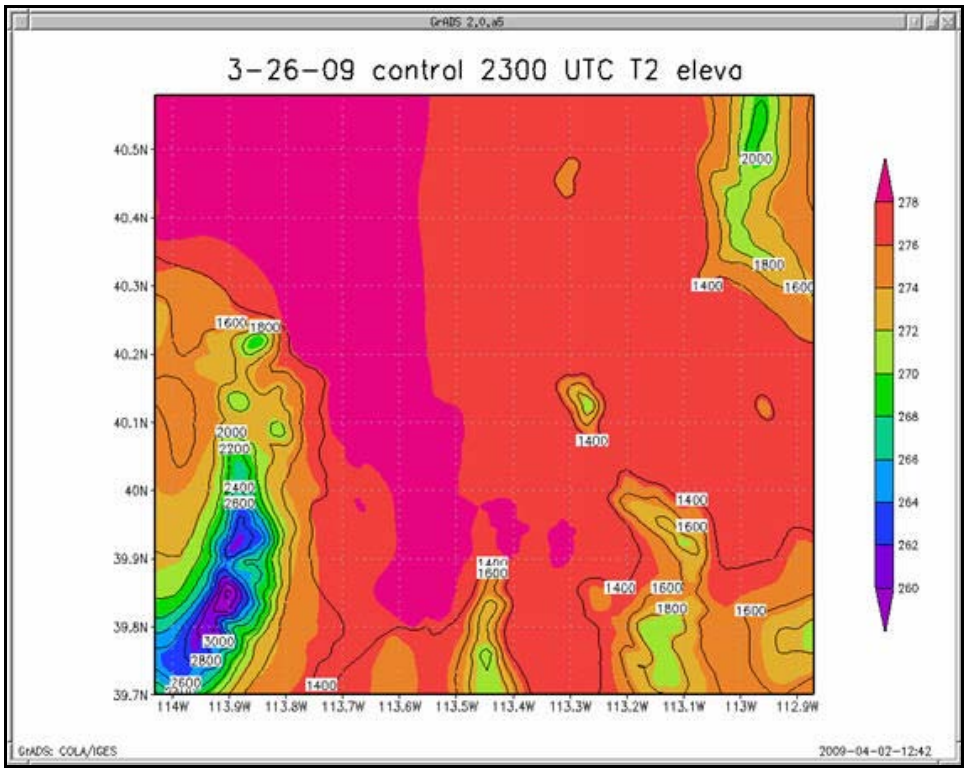

Figure 11. Surface temperature (T2) in K with terrain (contours) at 2300 UTC, 26 March 2009 over domain 2 for the control run.

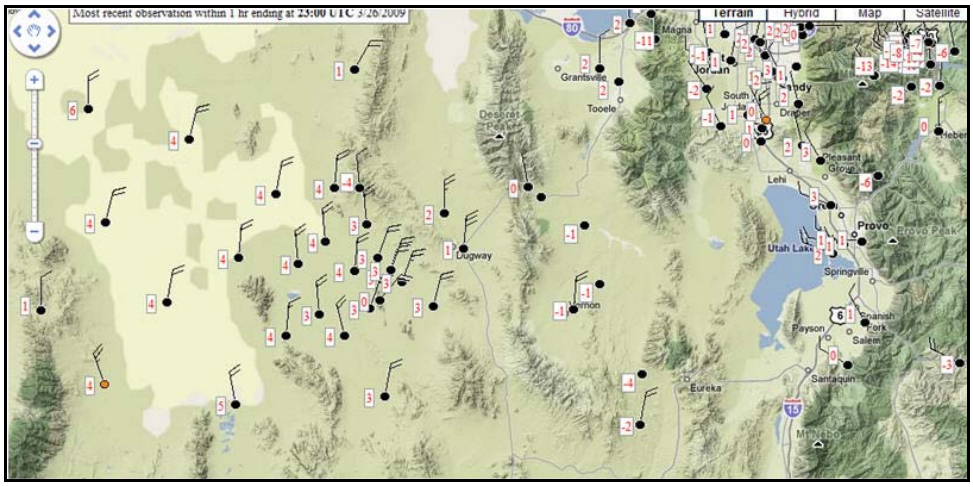

Figure 12. Surface temperature (°C) with wind direction at 2300 UTC, 26 March 2009 using Mesowest observations in domain area.

4.2 Case 2

Case 2: 21 April 2009 – This day featured a deep 534 dm upper low over Michigan with an upper ridge over the western United States, including the Utah area. The surface conditions were clear with light winds. The main purpose of this day was to study the basic terrain-induced wind circulations in the region on a day with no synoptic or dynamic interference.

At 1400 UTC, 21 April 2009 temperatures in the valley locations ranged from 6 to 9 °C, while higher surface temperatures (11–13 °C), were observed on the higher terrain or at the foothills of the mountains. A peak temperature of 15 °C was noted on the higher slopes to the southeast side of the grid. The observed winds were what might be expected for the early morning under a clear sky–nocturnal downslope or drainage winds off the higher terrain and a general south to north (downvalley) flow in the basin area. Given these observations, it could be assumed that there exists a strong temperature inversion, and this is verified by looking at the 1200 UTC SLC sounding (refer to figure 15), which indicates a 15.2 °C at 850 hPa.

4.2.1 Temperature and Wind field

Using the control run, the WRF overforecasts the surface temperature by approximately 3 °C as can be seen in figure 13. This overforecasting problem was not limited to the control run as can be seen in figures 16–19. In figure 17, the MYJ PBL was employed and shows a stronger bias to overforecast the surface temperatures with temperatures 4–5 °C higher than the observed. While the study size is still small, it appears that the MYJ PBL trended toward the highest temperature bias of all the model runs. The 80-level model (figure 18) and 40-level model (figure 19) runs both showed a bias of approximately 2–3 °C although the high-temperature bias was about 1°C over the basin areas. All models runs showed a light and variable wind pattern with weak circulations imbedded in the flow. None of these can be verified given their small size and lack

of higher resolution surface observations, although some areas of convergence can be seen in figure 14 in the northwest corner of the region and in two places near the higher terrain.

This tendency to have a bias in the temperature forecasts is not unique to just the 21 April case. The highest temperature error through this study was in the first six hours of the model simulation, which coincided with the overnight hours and early morning hours. Even more interesting is that the 21 April case had the largest statistical errors.

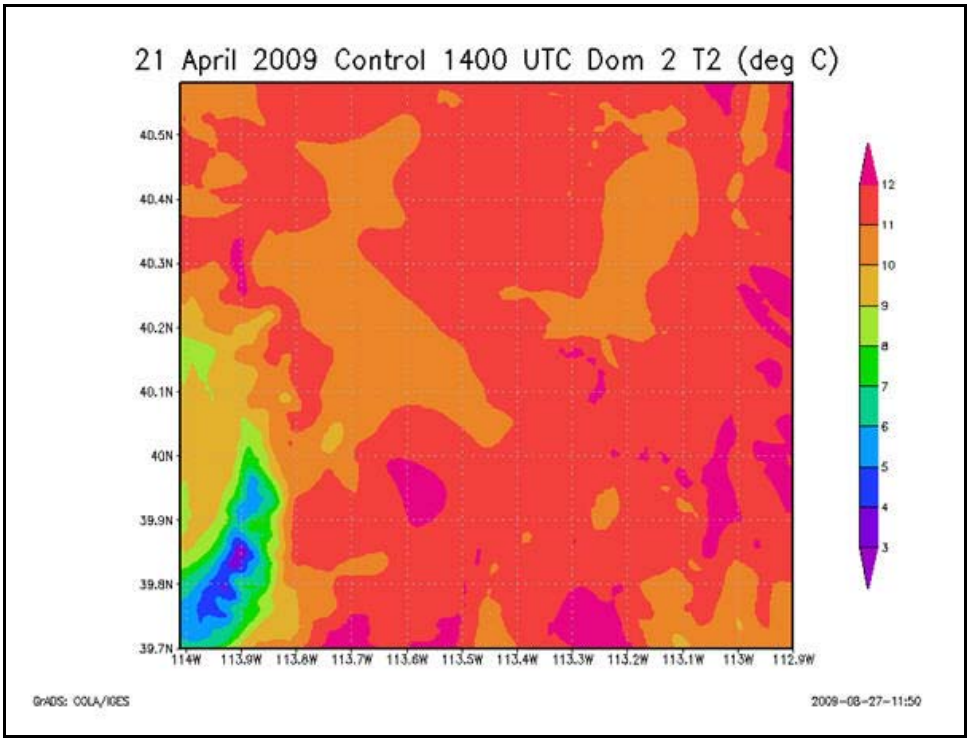

Figure 13. Surface temperature (°C) at 1400 UTC, 21 April 2009 over DPG grid (domain 2) for the control run.

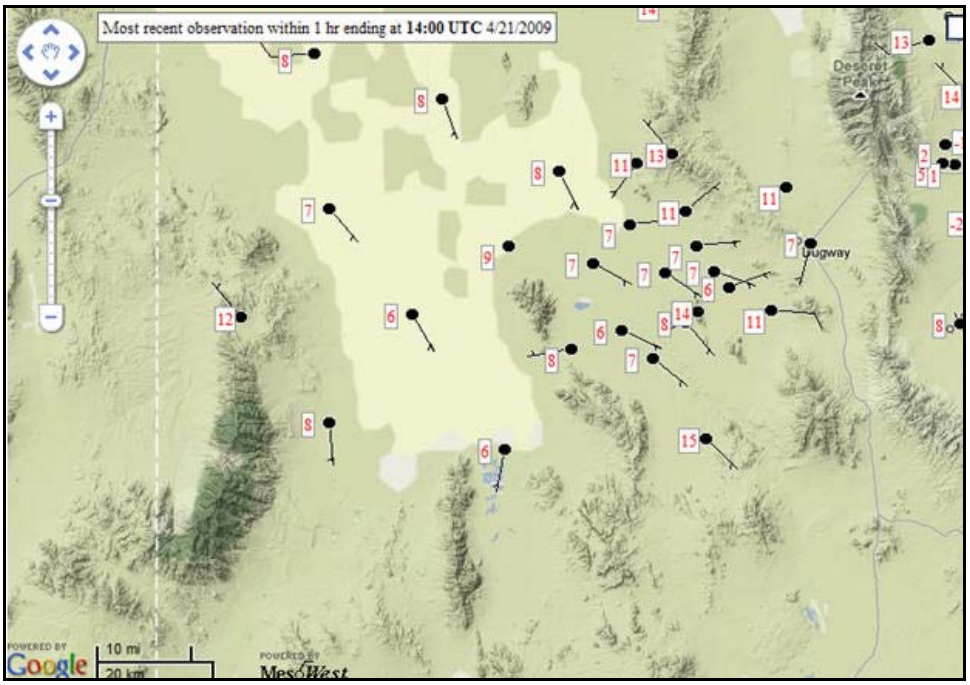

Figure 14. Observed temperature field (°C) at 1400 UTC, 21 April 2009 over domain 2.

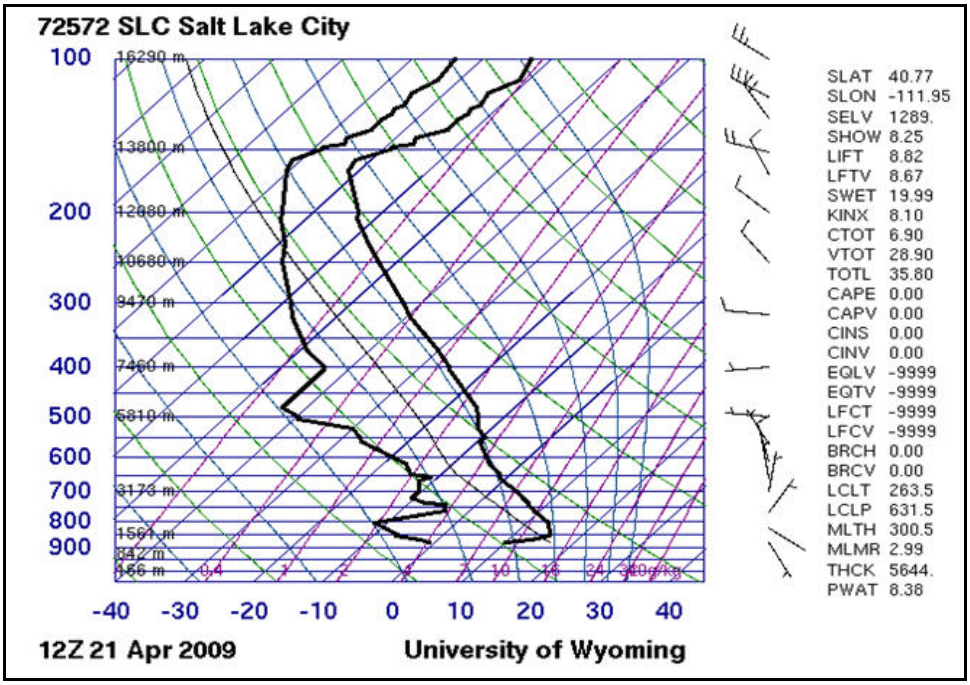

Figure 15. Upper-air observation at 1200 UTC at SLC 21 April 2009.

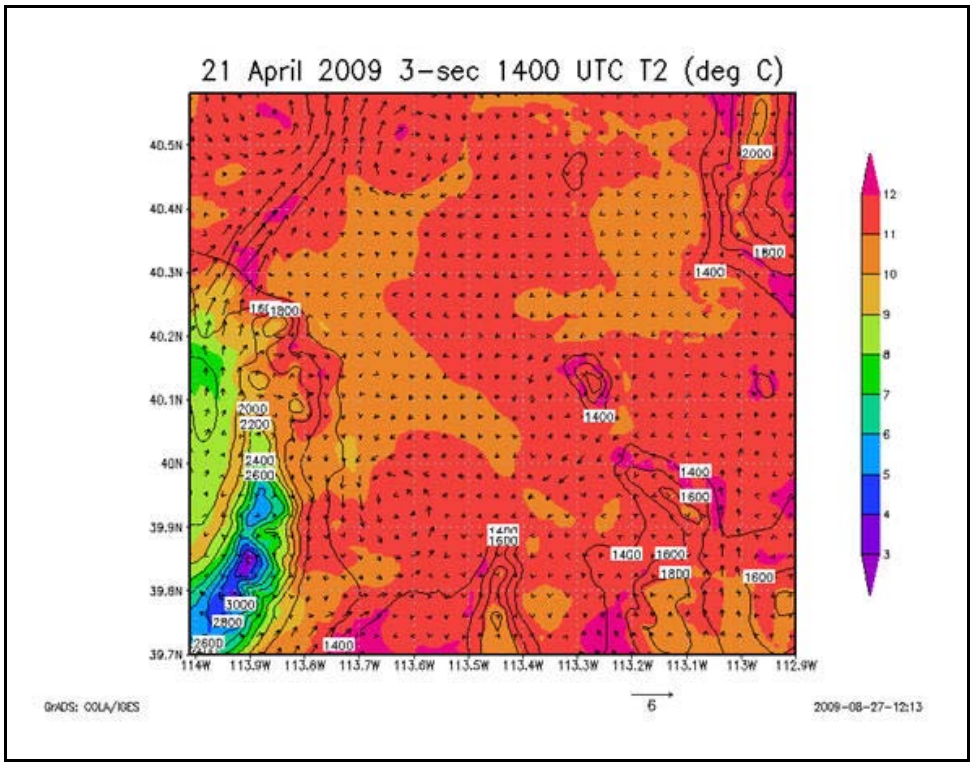

Figure 16. Surface temperature (°C) at 1400 UTC, 21 April 2009 over DPG grid (domain 2) for the model run with 3-second time step.

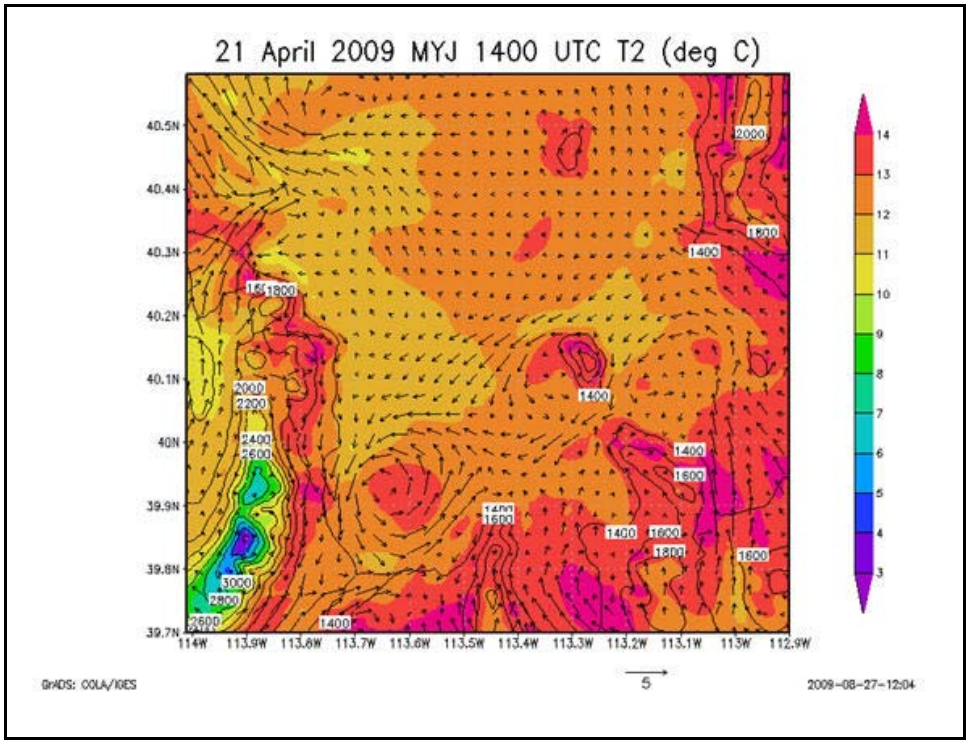

Figure 17. Surface temperature (°C) at 1400 UTC, 21 April 2009 over DPG grid (domain 2) for the model with MYJ PBL parameterization.

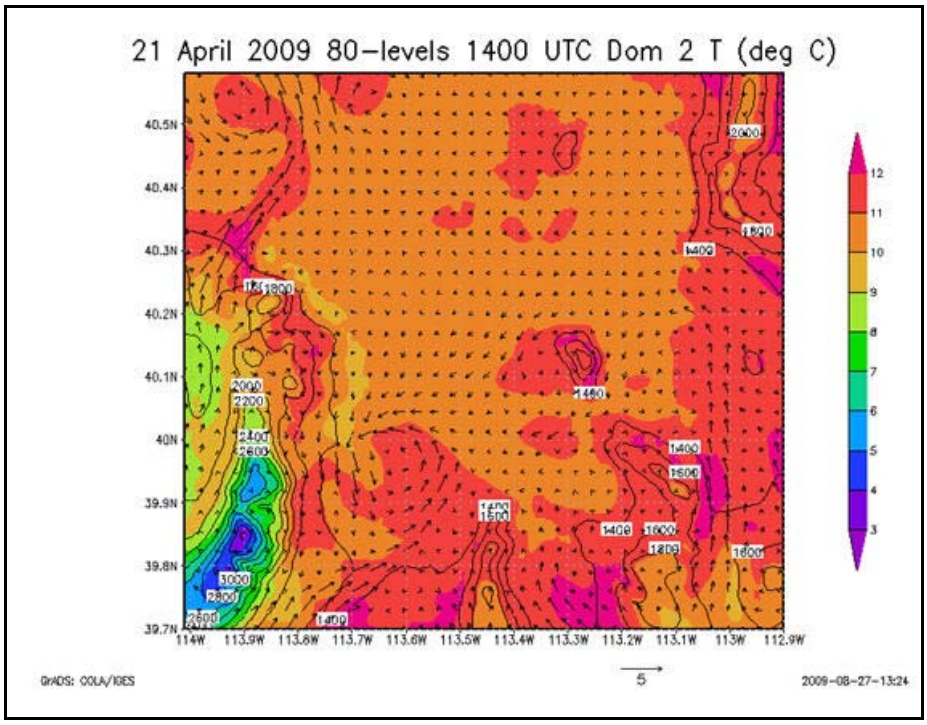

Figure 18. Surface temperature (°C) at 1400 UTC, 21 April 2009 over DPG grid (domain 2) for the model run with 80 vertical levels.

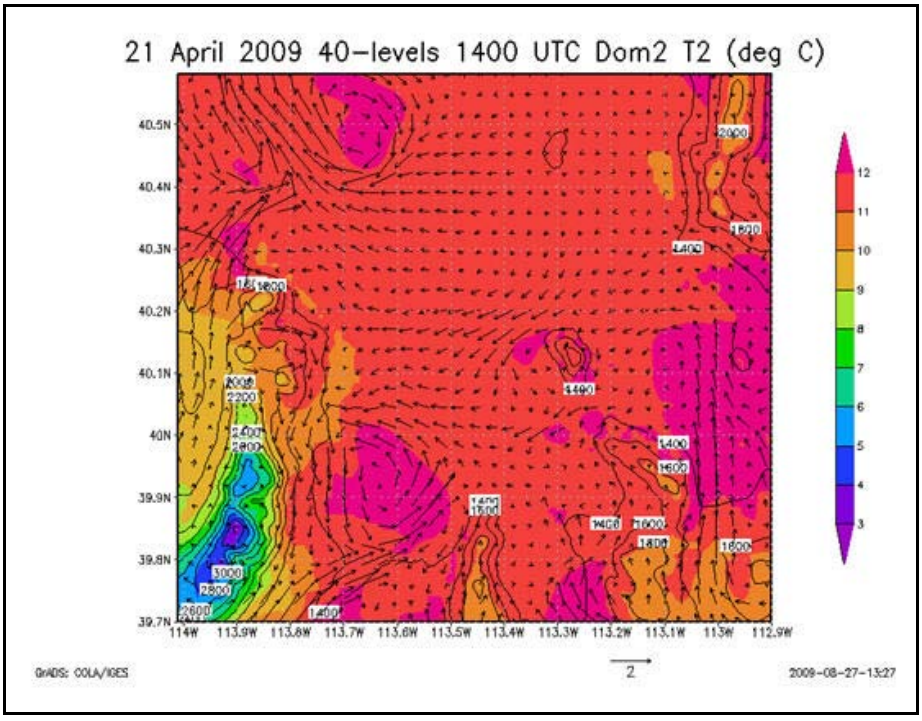

Figure 19. Surface temperature (°C) at 1400 UTC, 21 April 2009 over DPG grid (domain 2) for the model run with 40 vertical levels.

At 2300 UTC, temperatures had warmed to about 25 °C over much of the grid. Upslope winds were noted near the higher terrain and surface winds were from a northeasterly direction, perhaps influenced slightly by the Great Salt Lake.

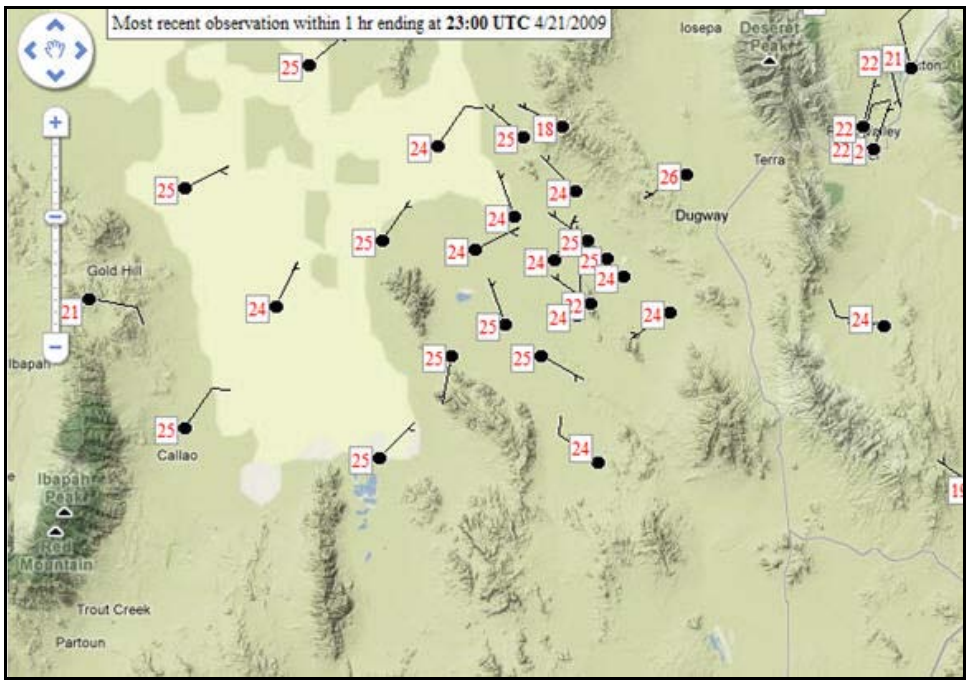

Figure 20. Surface temperature and wind directions observations over domain 2 at 2300 UTC, 21 April 2009 from Mesowest.

The model runs captured the general trends at 2300 UTC as seen in figures 21–24. The control run (figure 21) output matches well with the observed data. The surface winds are from the northeast across the western part of the grid, with a more northeasterly wind on the east side of the grid. The upslope winds are well depicted on the higher terrain with a general upvalley flow. The maximum temperatures in the basin are 25–26 °C, which agrees well with the SAMS data over the region. The other model runs displayed here agree with this; however, they do indicate a more easterly wind flow on the northern part of the grid. Otherwise, the temperature and wind fields are forecasted well.

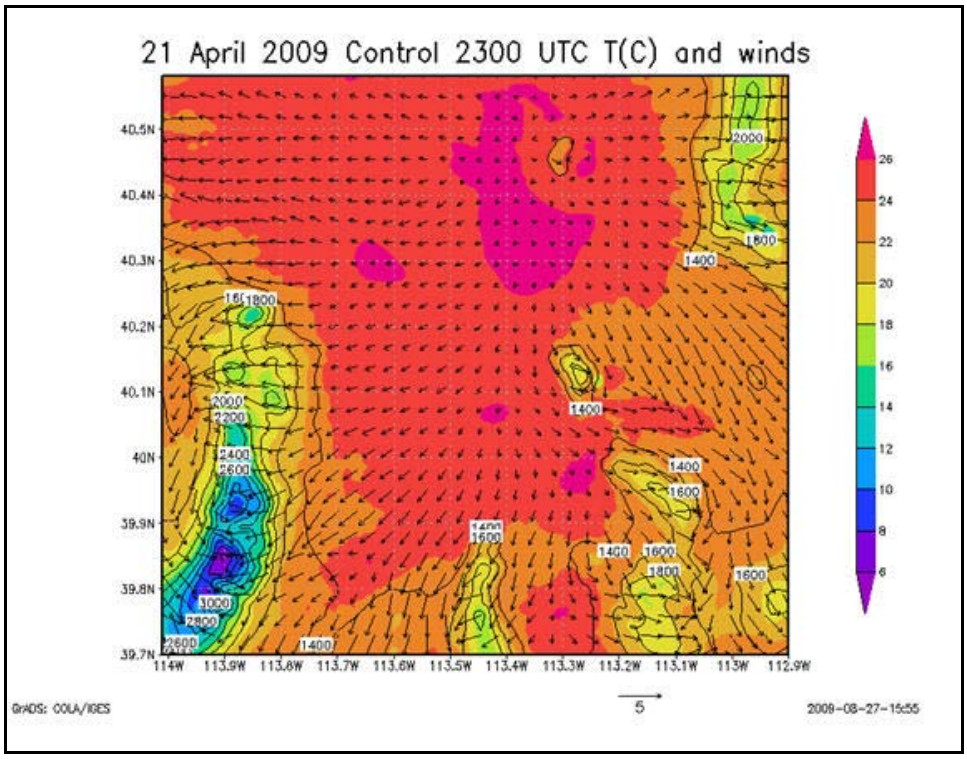

Figure 21. WRF surface temperature (°C) at 2300 UTC, 21 April 2009 over DPG grid (domain 2) for the control run of the model.

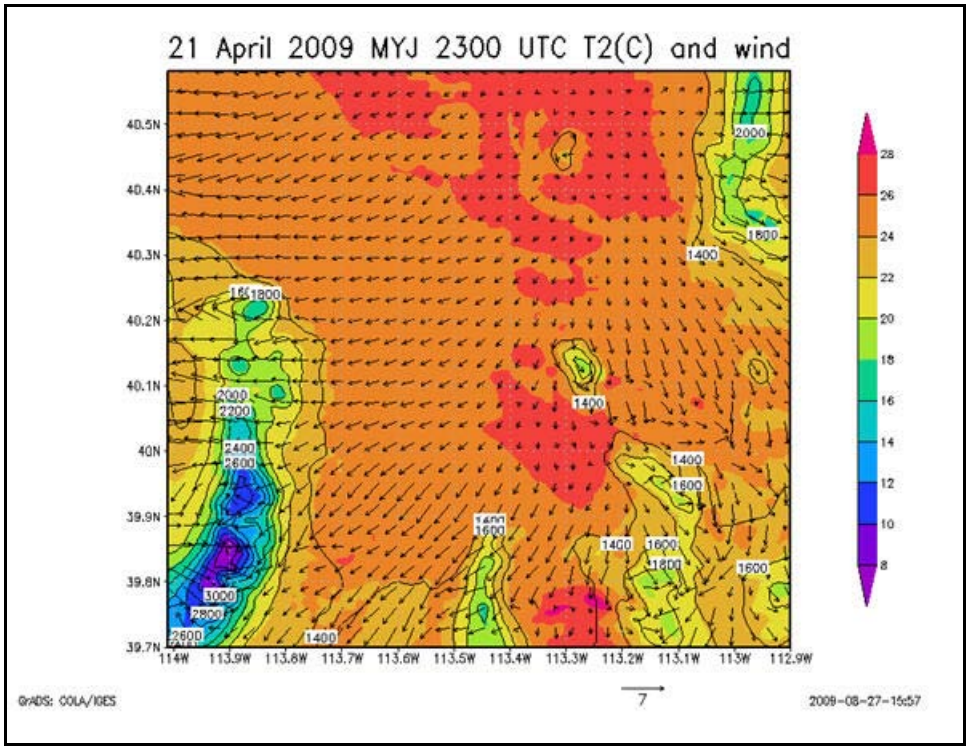

Figure 22. WRF surface temperature (°C) at 2300 UTC, 21 April 2009 over the DPG grid (domain 2) for model run using MYJ PBL.

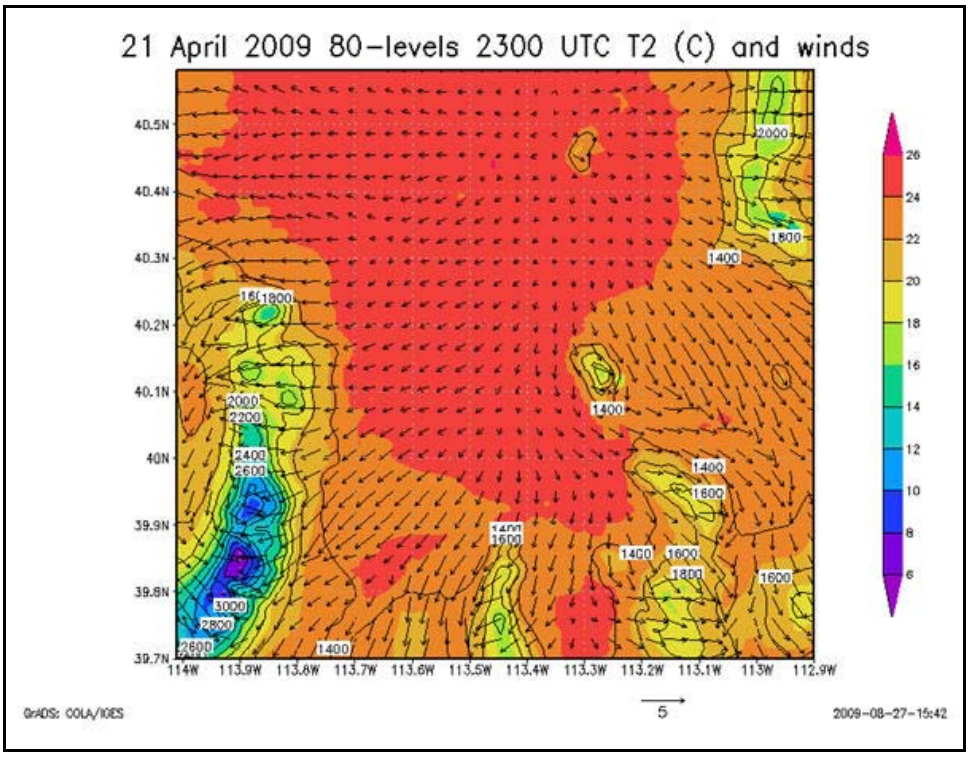

Figure 23. WRF surface temperature (°C) at 2300 UTC, 21 April 2009 over DPG grid (domain 2) for model run using 80 vertical levels.

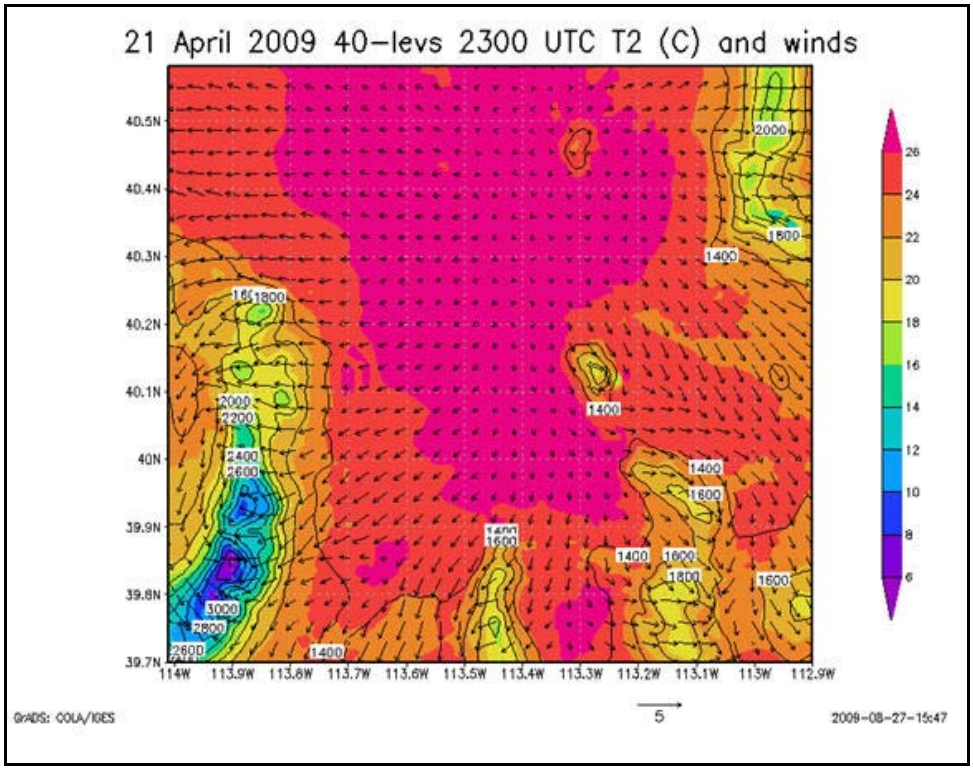

Figure 24. WRF surface temperature (°C) at 2300 UTC, 21 April 2009 over DPG grid (domain 2) for model run using 40 vertical levels.

4.2.2 Vertical Motions on the Boundary

An interesting phenomenon was noted along the southwest boundary of the inner domain when investigating the model vertical motion field. A strong area of upward vertical motion develops through the 24-h model cycle; however, it exists on model level 1 (etap) only, and appears only when using the two-way nest feedback option in the *namelist.input* file. It has been seen before for other modeling experiments run at ARL with past WRF-ARW versions, and is believed to be a fictitious artifact of the feedback option's interpolation and smoothing of heights and geopotential fields at the lateral boundary between parent and child nests. It seems to have no consequence on other model fields throughout the simulations. However, it does appear to be exponential as shown in figures 25–27 for the control run on 21 April 2009. While only the control run is shown here this vertical motion feedback feature did occur for all the model runs.

In figure 25, at 0800 UTC, there is light sinking motion or neutral vertical motion across the grid on a clear, calm night. At the far southwestern corner, there is an area of light rising motion to 0.6 m/sec. By 2000 UTC (figure 26) on 21 April, there is still generally weak sinking motion on the grid with some light rising motion over the higher terrain. However, along the boundary, motions of 5.5 m/sec are noted. In figure 27, by 0500 UTC, 22 April 2009 there are areas of light rising and sinking motions on the grid, but the area of rising motion has increased to 10 m/sec on the southwest border. Since it is difficult to see the small area of enhanced vertical motions, a closer view of this is provided in figure 28.

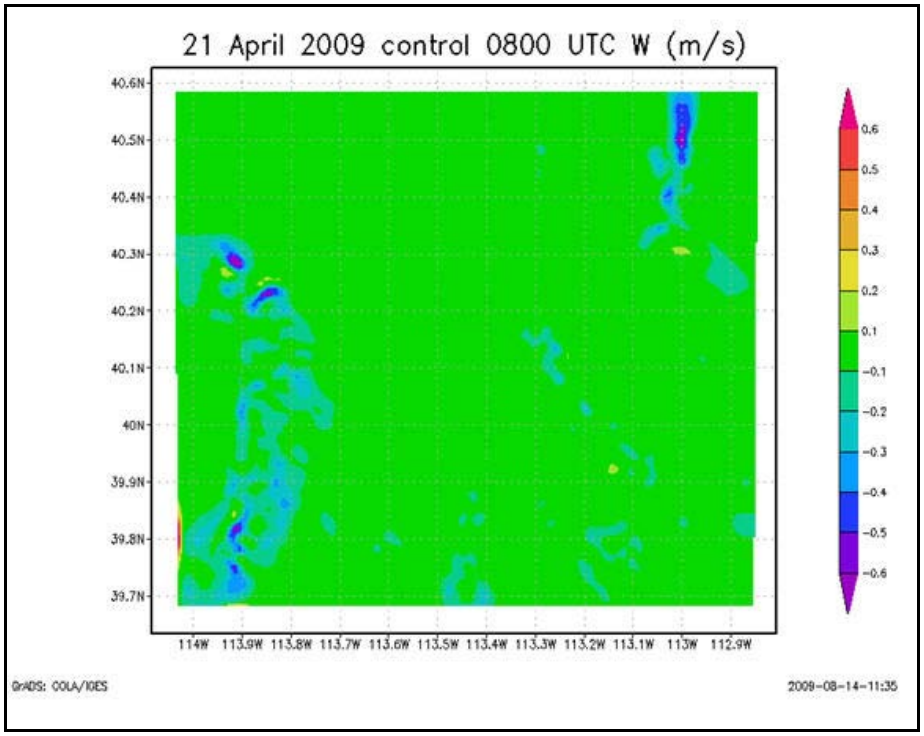

Figure 25. Domain 2 on 21 April 2009 with 0800 UTC level 1 vertical motions plotted.

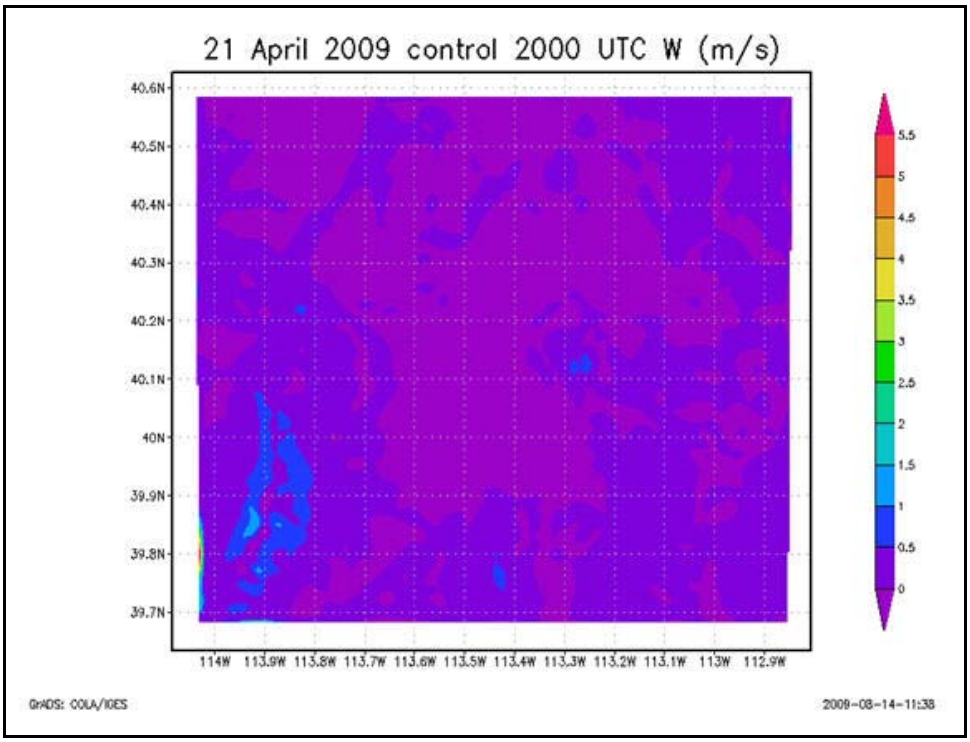

Figure 26. Model level 1 vertical motion field in m/s on 21 April 2009, 2000 UTC.

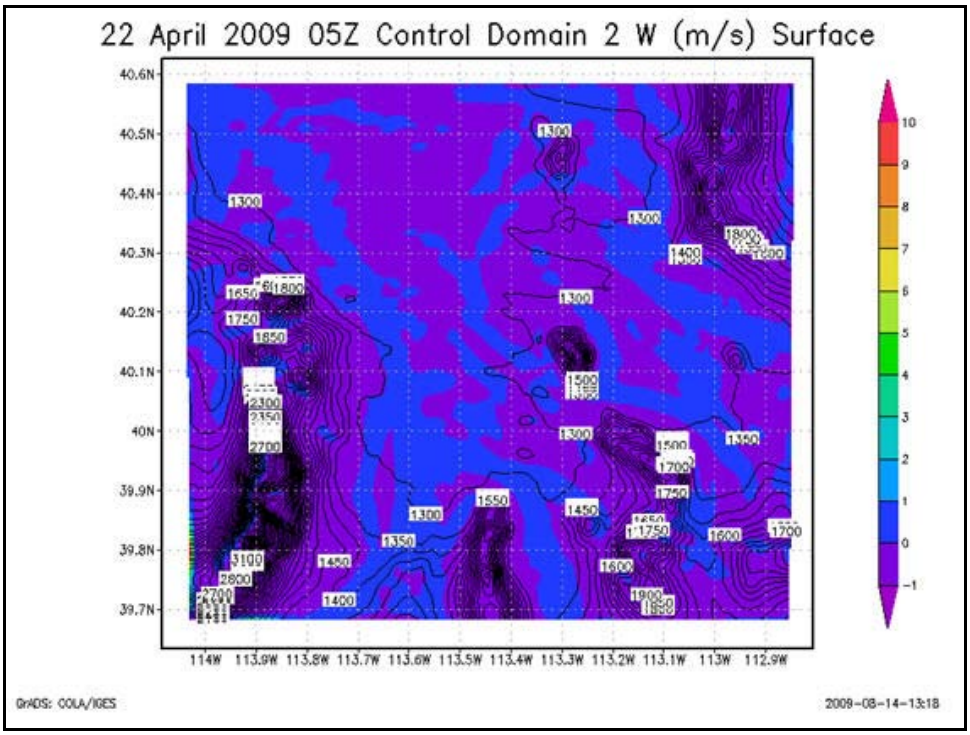

Figure 27. Vertical motion field at model level 1 in m/s on 22 April 2009, 0500 UTC .

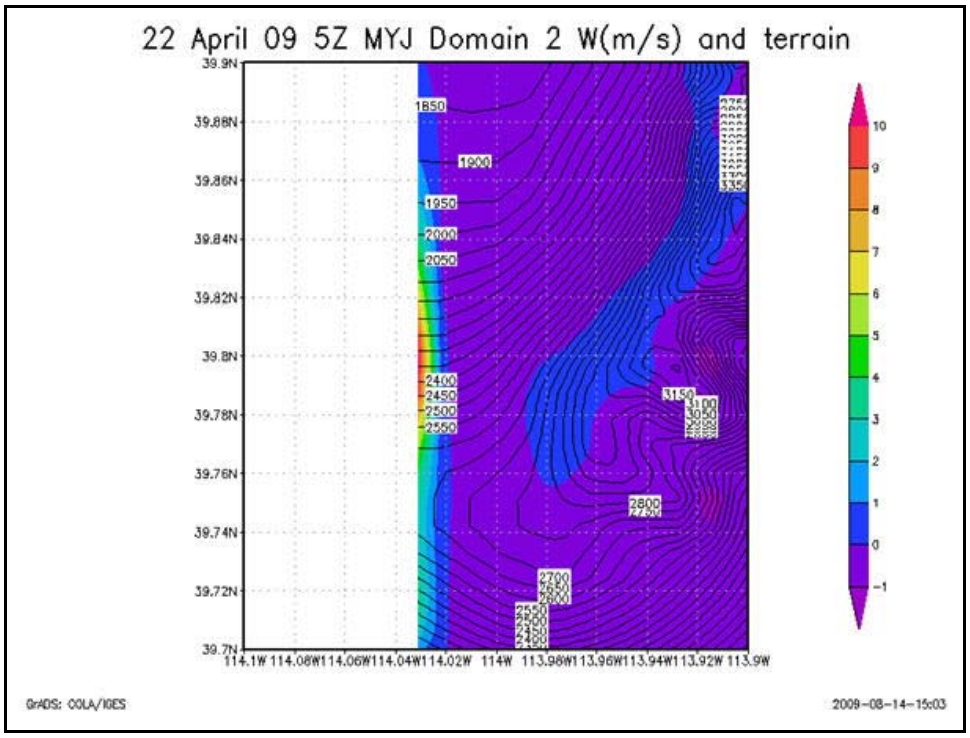

Figure 28. Close-up view of rising vertical motions on the border between the inner nest (domain 2) and parent nest (domain 1) at 0500 UTC, 22 April 2009 for the MYJ PBL run.

4.2.3 Short-wave Radiation and the *namelist.input* file

Another interesting discovery involved the short-wave radiation (model name SWDOWN) output. As displayed in figure 29, at 2300 UTC, 21 April 2009, the highest values of SWDOWN were noticed over the highest peaks of the Deep Creek Mountains on the southwest corner of the domain. There is a trend of higher values of SWDOWN over the peaks but the differences during the late afternoon hours were only 10–20 w/m^2. It was also interesting to note that the lowest values were forecasted to be to the northeast of the Deep Creek Mountains. On a sunny day such as this, it did not immediately make sense to see a difference of 50 w/m^2 over this area and at first it appeared that it was due to shading from the local mountain range. However, looking at some of the other model runs, this proved that it was not related to shading as seen in figure 30. The shape of the lowered SWDOWN area was different using microphysics option 2 than the control run, which would be impossible given that solar angle and terrain do not change from run to run of the model. In figure 30, the shading area was aligned north to south and closer to the mountain range than the area in figure 29, which is displaced further downstream from the mountain range. The situation became even more problematic when looking at the case of microphysics 8. Using that parameterization, the shading area near the highest terrain did not exist as shown in figure 31. This required even more study and it was discovered that for domain 2 the shading option in the *namelist.input* file, the model control and parameterization

file, was not even turned on. While this oversight was attributed to an error in the WRF Users Guide not mentioning that this variable must be declared for both domain 1 and domain 2, it did not explain why the different physics routines still had different values for SWDOWN.

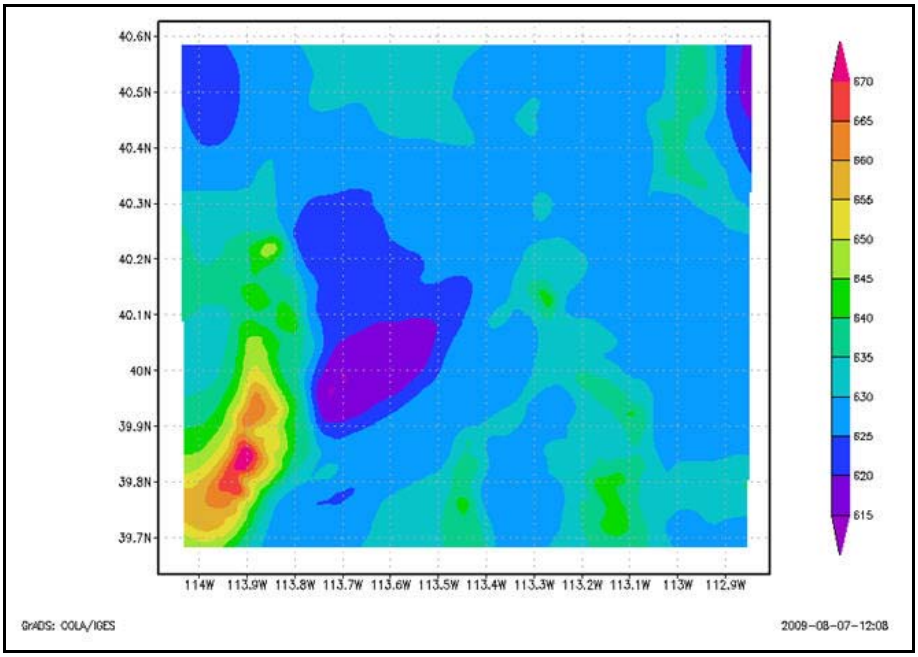

Figure 29. Plot of short-wave radiation (w/m^2) for 21 April 2009 at 2300 UTC over domain 2 for control run of the WRF-ARW.

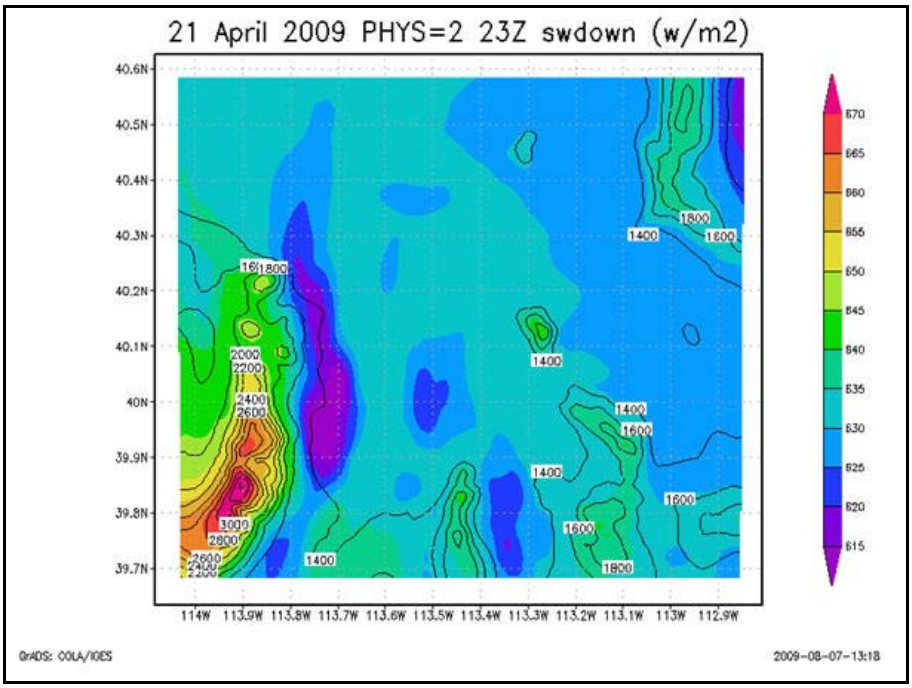

Figure 30. Plot of short-wave radiation (w/m^2) for 21 April 2009 at 2300 UTC over domain 2 for model run using microphysics option 2.

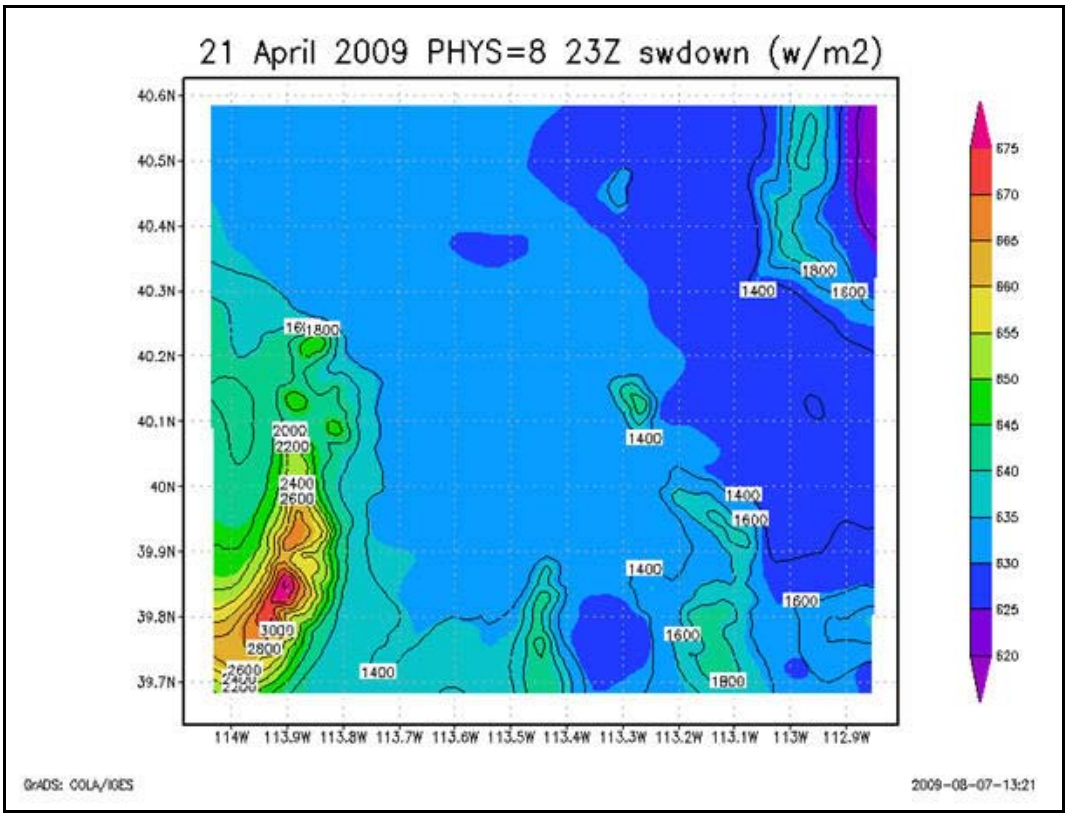

Figure 31. Plot of short-wave radiation (w/m^2) for 21 April 2009 at 2300 UTC over domain 2 for model run using microphysics option 8.

Thus, an investigation of the moisture parameters and vertical motion in the model output was conducted. These parameters included qsnow, qvapor (water vapor mixing ratio), qcloud (cloud water mixing ratio), qrain, qice, W (z-wind component), and RH. There was little dissimilarity in many of these fields. No qcloud was produced nor was there any qrain generated on any of the model runs. Additionally, there was no precipitation forecasted at any time in any of the model runs. It was noted that a layer of higher RH was forecasted in all model runs between 12 and 13 km MSL. The highest forecasts of RH were 60% in this layer. The only variable with some variation between the different model simulations was qice. As an example, in figure 32, the plot of qice for the control run at 40.0N (looking east-west across the grid). It shows a layer of qice being forecasted around 12 km MSL, which coincides with the higher RH area. Qice in microphysics option 8 is shown in figure 33. The concentration of qice is an order of magnitude less than the control run and also a much smaller area. It was concluded that these values of qice were the actual cause of the slight reduction in SWDOWN seen in the control run and most of the other model runs. However, the lack of qice might be the reason why the model run using microphysics option 8 did not produce a reduction in SWDOWN. Additionally, this influence of qice on SWDOWN did not exist until 2200 UTC. The presence of qice continued through the remaining hours of the model run until 0600 UTC, 22 April 2009, but SWDOWN was only

observed until 0100 UTC when the sun set on the grid and the influence of qice appeared to be minimal at that point in the control run.

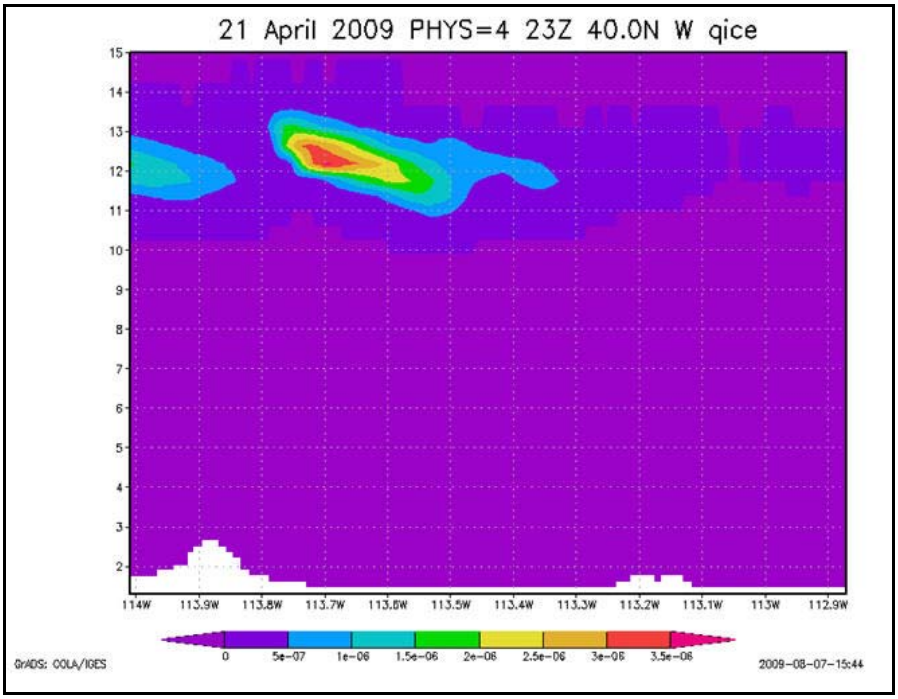

Figure 32. East-west plot of qice 21 April 2009 at 2300 UTC at 40.0N over domain 2 for model run using microphysics option 4, the control run.

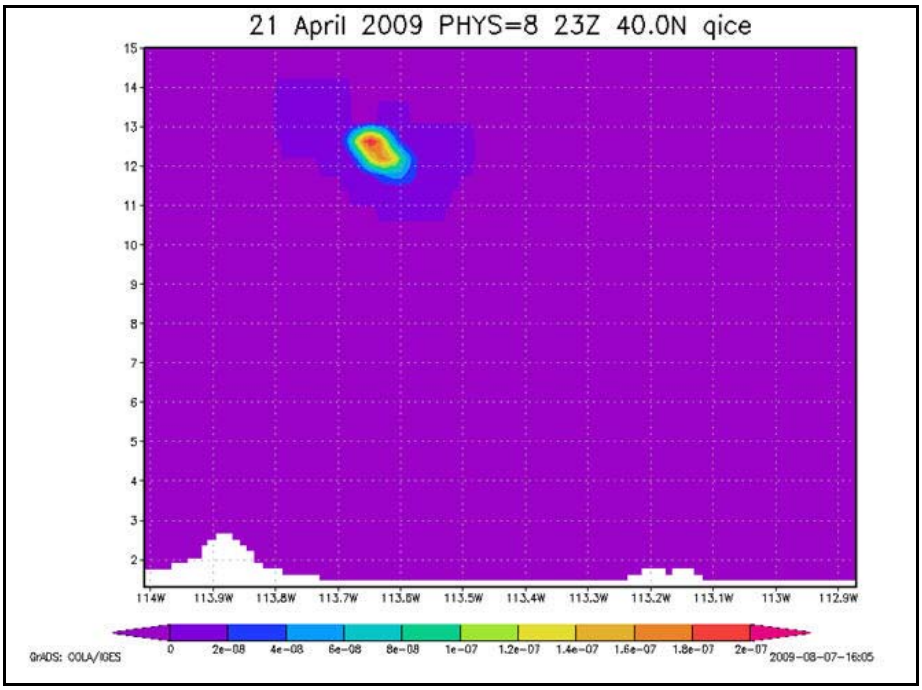

Figure 33. East-west plot of qice 21 April 2009 at 2300 UTC at 40.0N over domain 2 for model run using microphysics option 8.

As an experiment, the control run was performed with the correct changes to the *namelist.input* file, which properly "turned on" the slope-rad and topo-shading terms. The results can be seen in figure 34 and they illustrate more realistic values of SWDOWN. Areas just east of the terrain have a reduction of SWDOWN at 2300 UTC of over 100 w/m^2. The same influence was detected in the morning hours when the sun was rising or lower in the eastern sky, and SWDOWN was reduced on the west side of the mountain ranges.

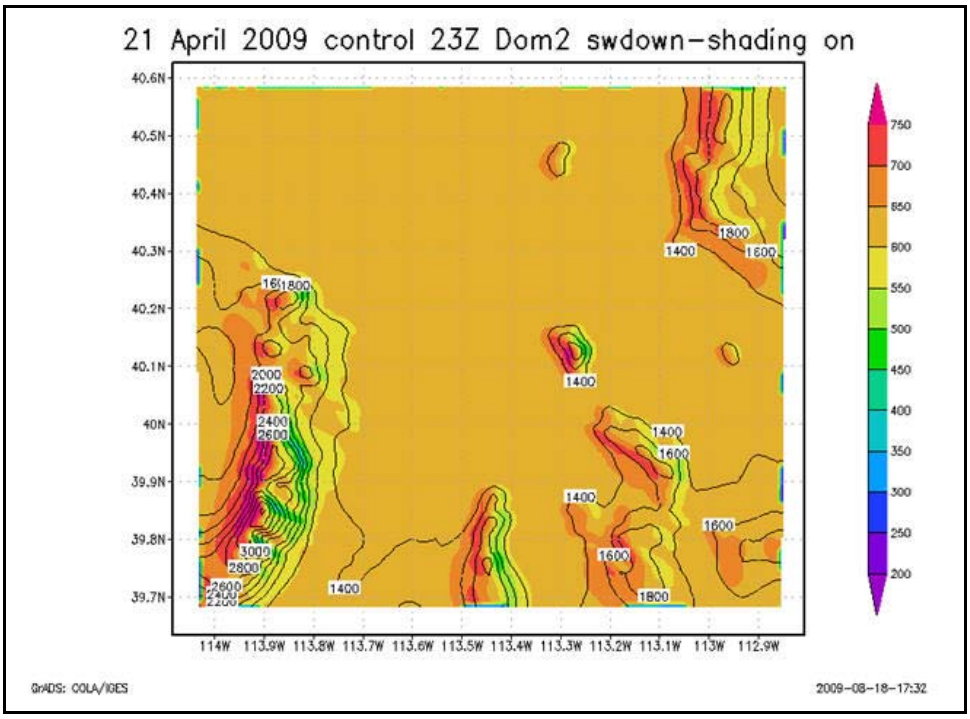

Figure 34. Plot of short-wave radiation (w/m^2) for 21 April 2009 at 2300 UTC over domain 2 for control run (microphysics=4) with slope_rad and topo_shading turned on for domain 2.

The plot in figure 34 also introduced another interesting effect on the boundary of domain 2. While it is difficult to see on the figure, significant drops of SWDOWN of over 500 w/m^2 are noted along the boundary. This appears to be a similar problem to the excessive vertical motion found on the southwest side of the grid when the feedback option is turned on in the *namelist.input* file. There is evidence that this also happens when plotting T2 (surface temperature at 2 m above ground level [AGL]), TH2 (potential temperature at 2 m AGL), and Td (surface dew point). The problem is not seen after SWDOWN is off, when there is no solar input

4.3 Case 3

The 19 May 2009 case was another complicated case even without the influence of any large-scale weather influence. There was a strong upper high over Oklahoma at 1200 UTC, 19 May 2009 with a 546 dm upper-low over southwest British Columbia, Canada. At the start of the forecast period there was weak southwest flow aloft. At the surface level there was a low

pressure center in southeast British Columbia with a cold front to northwest California. The 1200 sounding is shown in figure 35.

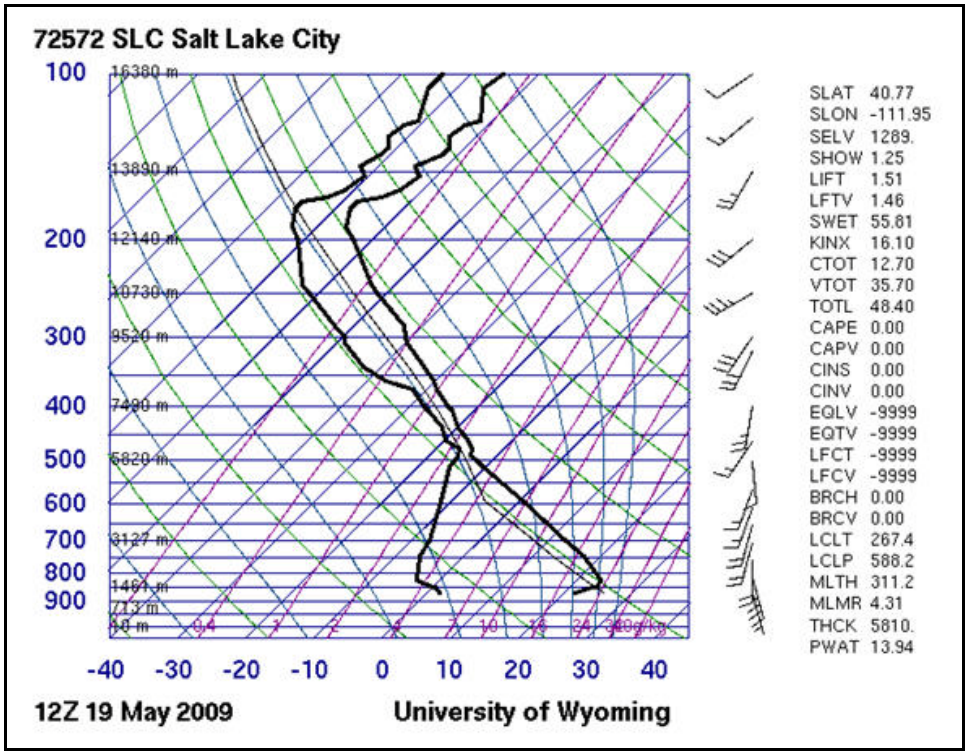

Figure 35. Upper-air observation at 1200 UTC, 19 May 2009 for SLC, UT.

The morning sounding shows a moist layer from 500 hPa to 350 hPa, with a deep dry layer below that. Winds are generally from the south in the low and middle layers with a more westerly component in the higher levels. At 1400 UTC, surface observations available at the time reported ceilings of between 14000 and 20000 feet AGL over Utah, with south surface winds. This led to an unseasonably warm night in the region, given the cloud cover and winds. The local observations from the SAMS data at 1400 UTC is shown in figure 36. The control run of the model is shown in figure 37, with the wind flow and temperature (°C). Similar to the case of 21 April, the forecasted temperature at 1400 UTC is 2 °C warmer than the observations for the control run. The run using the MYJ boundary-layer parameterization (not shown) also indicates a forecast about 2 °C warmer than observed.

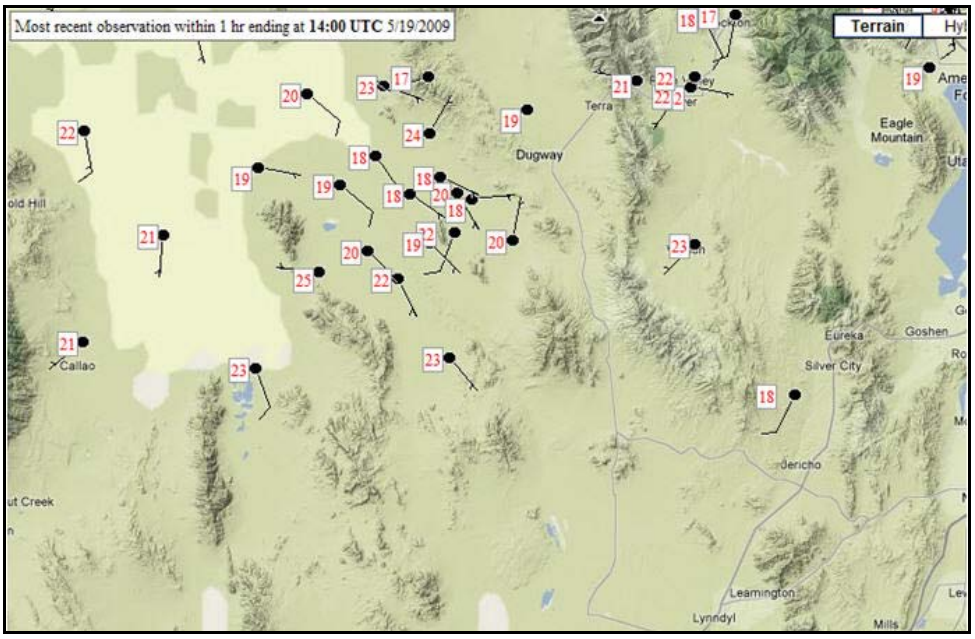

Figure 36. Temperature (°C) and winds over DPG area at 1400 UTC, 19 May 2009.

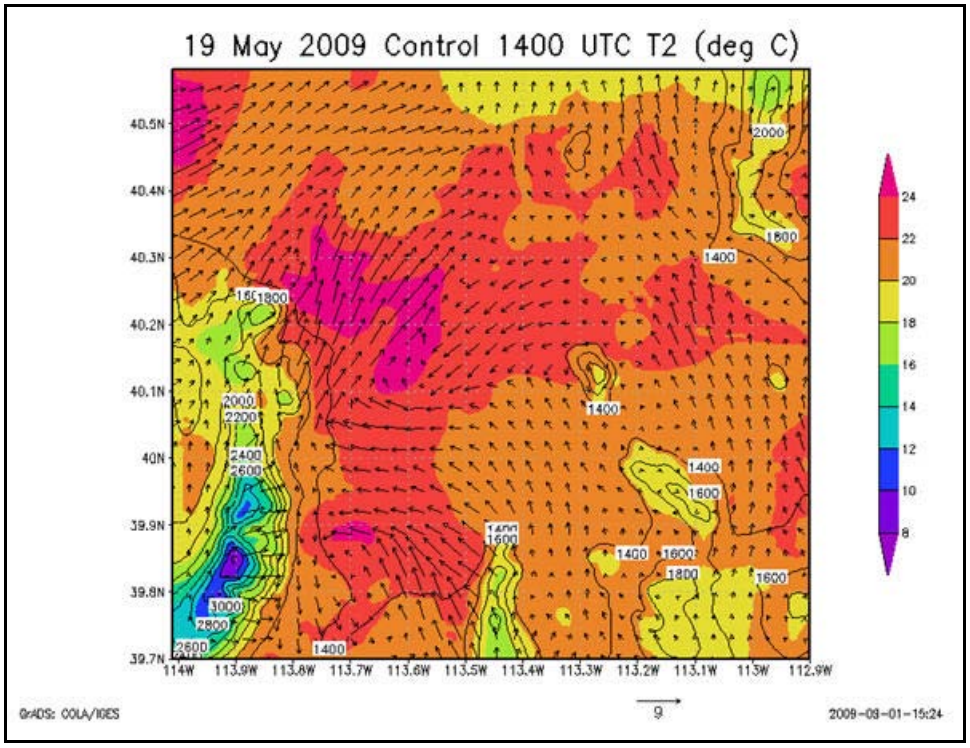

Figure 37. WRF model output of temperature (shaded in °C) and wind field for 1400 UTC, 19 May 2009 for the control run.

Analysis of the model runs at 2300 UTC showed another interesting case of the SWDOWN variable and the relationship with the upper-air moisture fields. Figure 38 shows the SWDOWN field for the control run. The model has isolated streak-like regions where SWDOWN is only

150–200 w/m^2 just a few kilometers from areas of 600 w/m^2. While this can be realistic, it became necessary to investigate the cause of these wide differences over short distances.

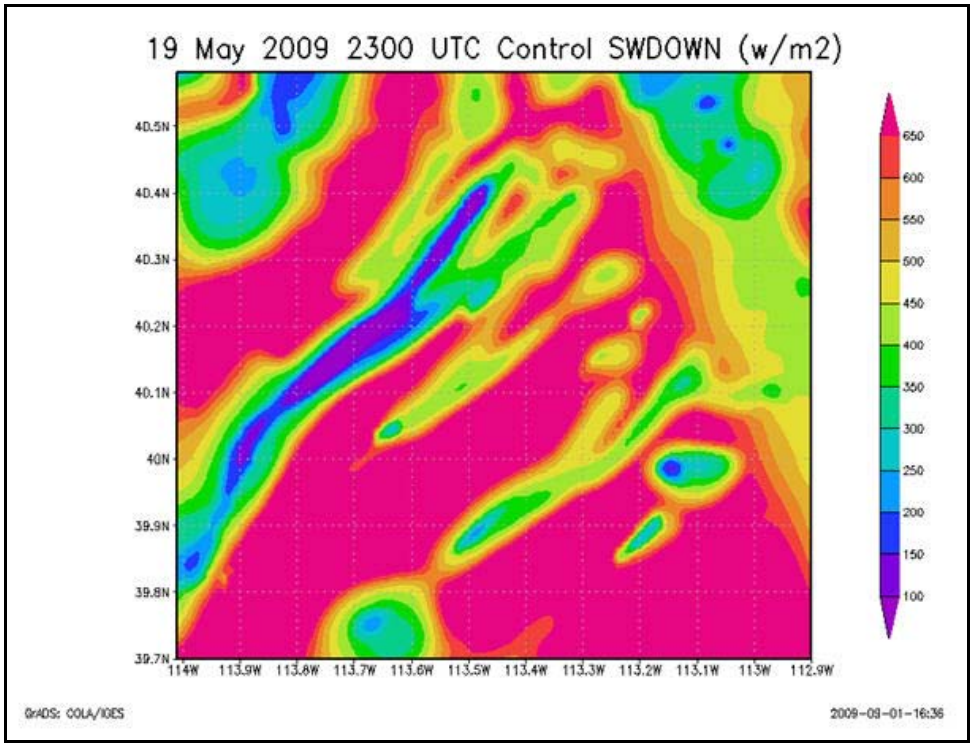

Figure 38. WRF model output of SWDOWN (w/m^2) field for 2300 UTC, 19 May 2009 for the control run.

At etap level 25, a significant amount of mid-level moisture was found. It can be seen that this higher RH coincides well with the decrease of SWDOWN at the surface as displayed in figure 39. While this result is not unexpected, when looking at the qice, the wind field and the vertical motion field, it was found that all these parameters combined to cause the decrease in SWDOWN. In figure 40, the wind field appears to be divergent in the areas of rising vertical motion, which also agrees with the rapid decrease of SWDOWN at the surface. A final intriguing point of interest in this part of the study was the qrain field at level 25. As shown in figure 41, the temperature field where the qrain is forecasted indicates temperatures as low as –10 °C at that level. Apparently, the model produces rainwater at temperatures well below 0 °C.

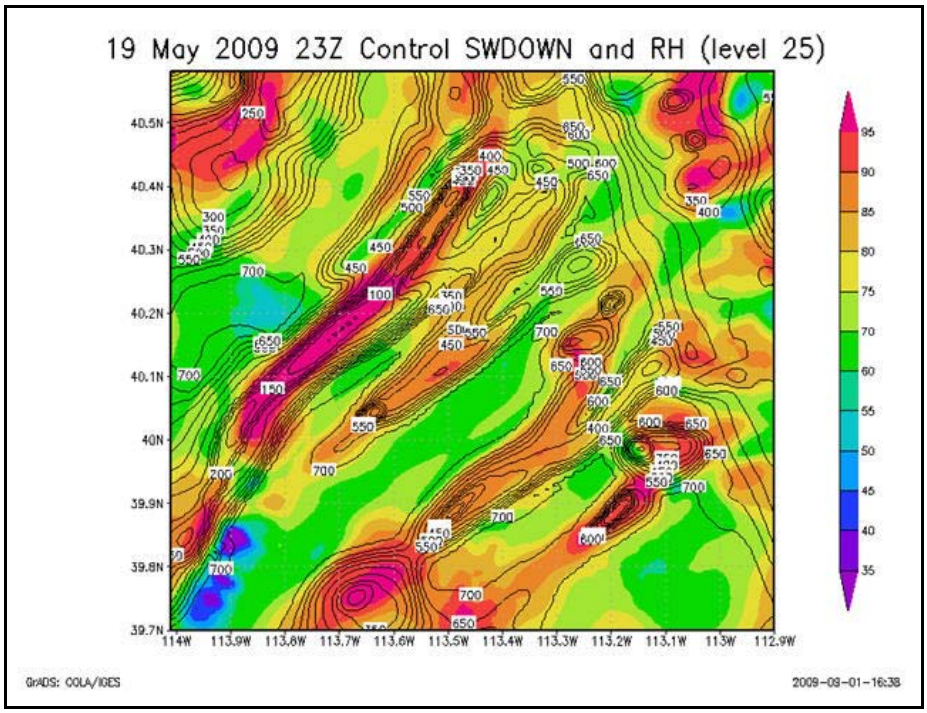

Figure 39. WRF model output of SWDOWN (contours in w/m^2) field in contours for 2300 UTC, 19 May 2009 for the control run along with the RH (shaded in percent) at level 25 of the model.

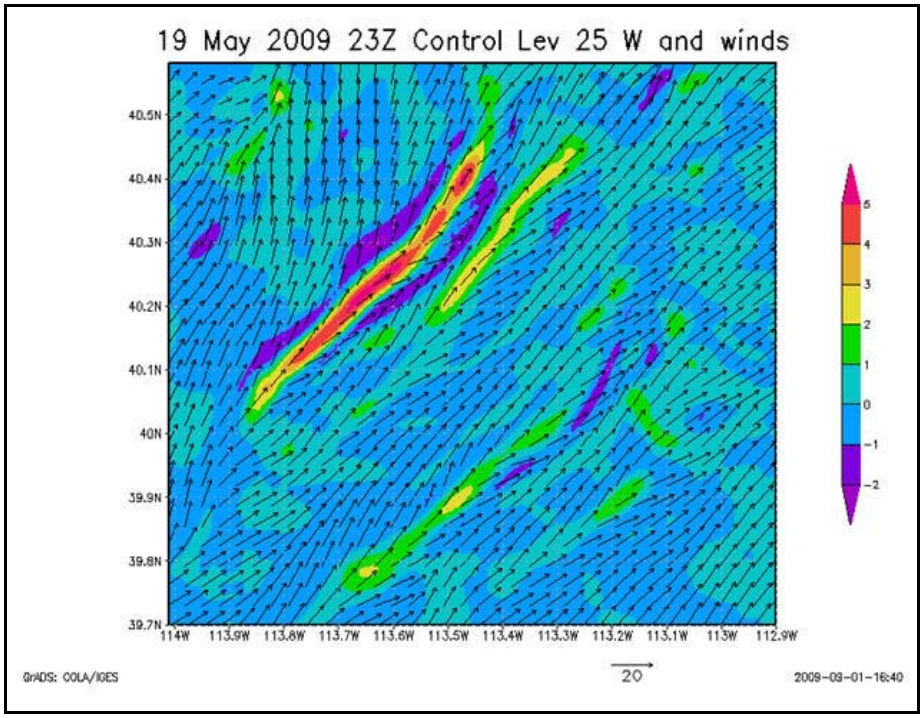

Figure 40. WRF model output of vertical motion (shaded in m/sec) at 2300 UTC, 19 May 2009 for the control run along with wind vectors at level 25 of the model.

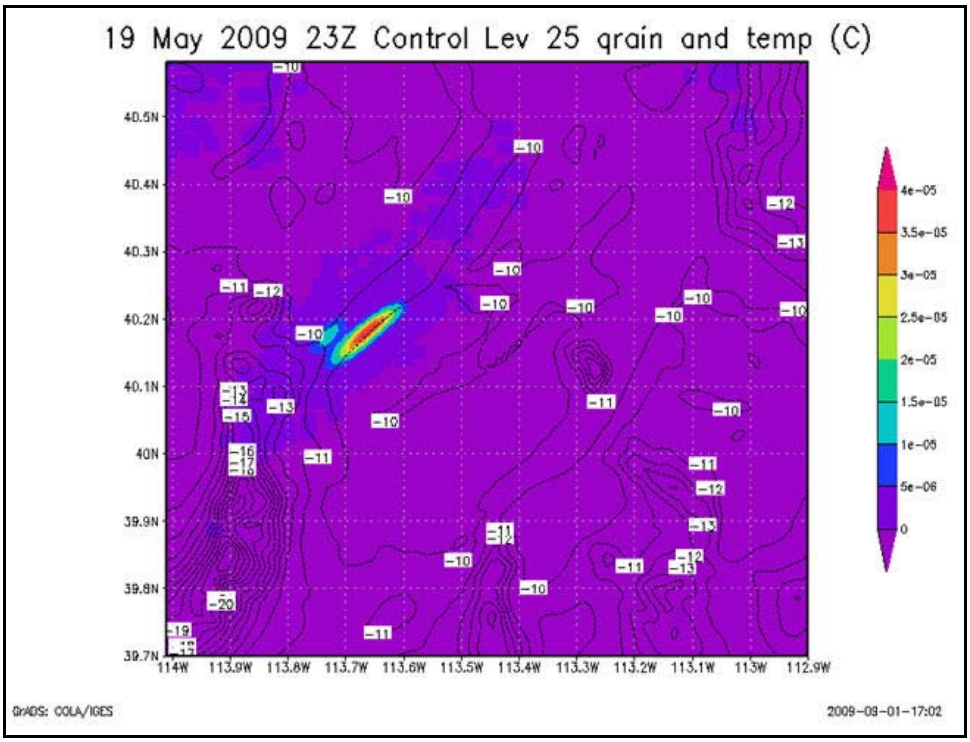

Figure 41. WRF model output of the qrain (shaded) field at 2300 UTC, 19 May 2009 for the control run along with temperature contours (°C) at level 25 of the model.

The surface pressure field is often overlooked as a parameter in model verification and validation. However, statistical evaluation for the 19 May case indicates a large pressure error during the afternoon hours centered at 0000 UTC. The RMSE for the surface pressure was nearly 5.00 hPa. In figure 42, the forecasted surface pressure field is plotted for 0000 UTC, 20 May 2009, while in figure 43 the observed SAMS pressure and wind field is shown. It can be seen that the average forecasted pressure is 1002–1003 hPa in the basin, while the observed values are shown to range from 997.3 to 999.0 hPa with some higher values on the western side of the grid. It is uncertain why this occurs, but earlier in the day at 1200 UTC (not shown) pressure differences were only about 1–2 hPa.

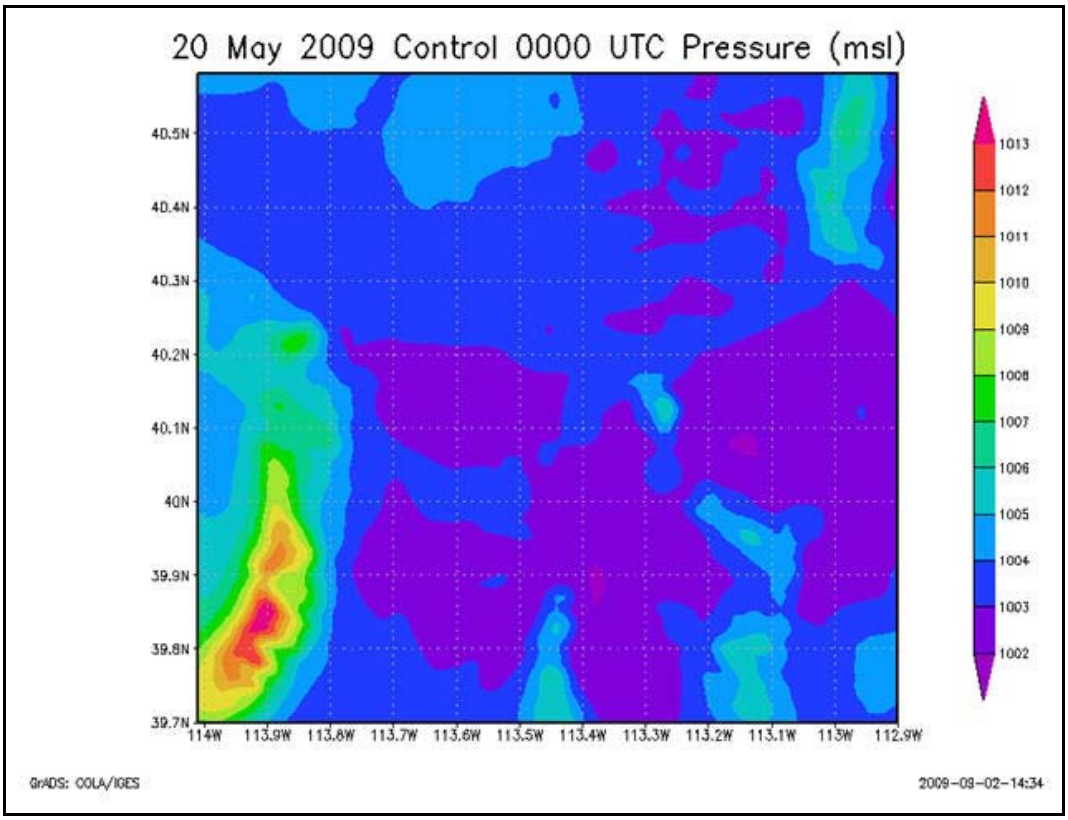

Figure 42. WRF model output of the surface pressure (hPa) field at 0000 UTC, 20 May 2009 for the control run.

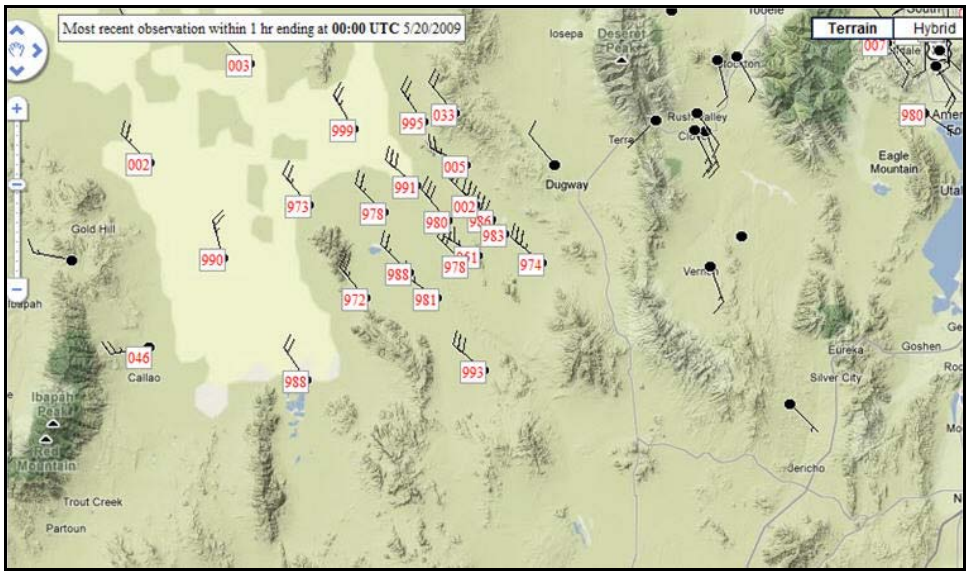

Figure 43. Observed surface pressure (hPa) field and surface wind observed at 0000 UTC, 20 May 2009 over the DPG grid (domain 2).

4.4 Case 4

The upper-air map showed a strong upper ridge over Oklahoma with a trough axis from eastern Washington to western Nevada. This put Utah in a moderate southwest flow aloft with winds from 225 degrees at 37 knots at 500 hPa with low-level winds from the south.

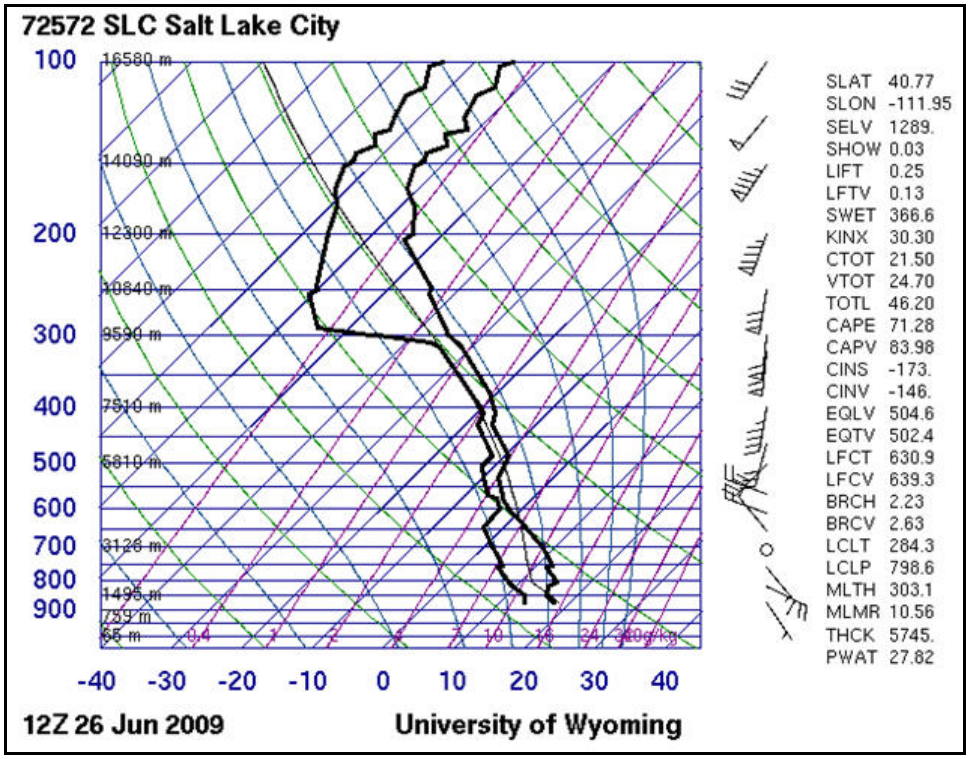

Figure 44. Upper-air observation at SLC 1200 UTC, 26 June 2009.

The sounding is moist for the time of year and it features a combination of "monsoonal" moisture along with the influence of the upper-level trough moving through the region. As expected the models did generate areas of convection during the 24-h model run initiated at 0600 UTC, 26 June 2009. One feature of the day was that drier air moved into the region during the day as the trough passed to the north, thus, shifting the winds to a weaker northwesterly flow along with mixing drier air to the boundary layer. Most of the rainfall was over by late in the afternoon. Table 4 shows the rainfall in certain regions of the grid for each different model simulation. In the table it can be seen that there is a wide variation in rainfall from model simulation to model simulation with the highest rainfall associated with the microphysics 8 option and 3-sec time steps. The lowest rainfall amounts occur with the control run (microphysics 4) and microphysics 2 options. In most of the grids, the heaviest rainfall amounts occur in the southeast corner of domain 2 with the lowest rainfall forecasted in the highest terrain in the southwest region of the grid. Figures 45 and 46 show two examples of the rainfall amounts for the 80-level case and microphysics 8 option.

Table 4. Precipitation amounts (mm) for various regions of the grid on 26 June 2009 for each of the seven model simulations.

Model Simulation	Maximum Precipitation on the Grid (mm)	Southeast Corner Area (mm)	Northwest Corner Area (mm)	Highest Precipitation over Deep Creek Mountains (mm)
Control Run (microphysics=4)	11.4	11.4	8.1	10.2
Microphysics=2	12.7	11.4	12.7	7.6
Microphysics=8	25.4	27.9	16.5	0.0
MYJ PBL	14.0	14.0	9.7	8.9
40-level simulation	20.3	20.3	3.8	3.8
80-level simulation	22.9	22.9	8.9	6.4
3-second time steps	27.9	27.9	8.9	8.9

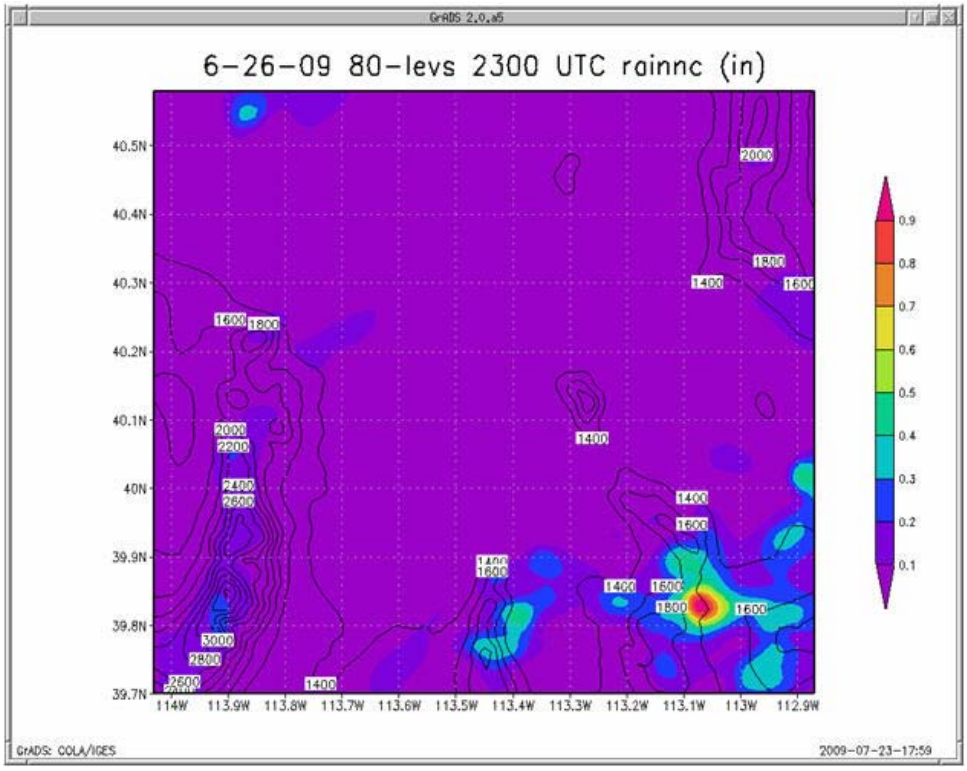

Figure 45. Rainfall totals (mm) at 2300 UTC for the 26 June 2009 model run using 80 levels in model run.

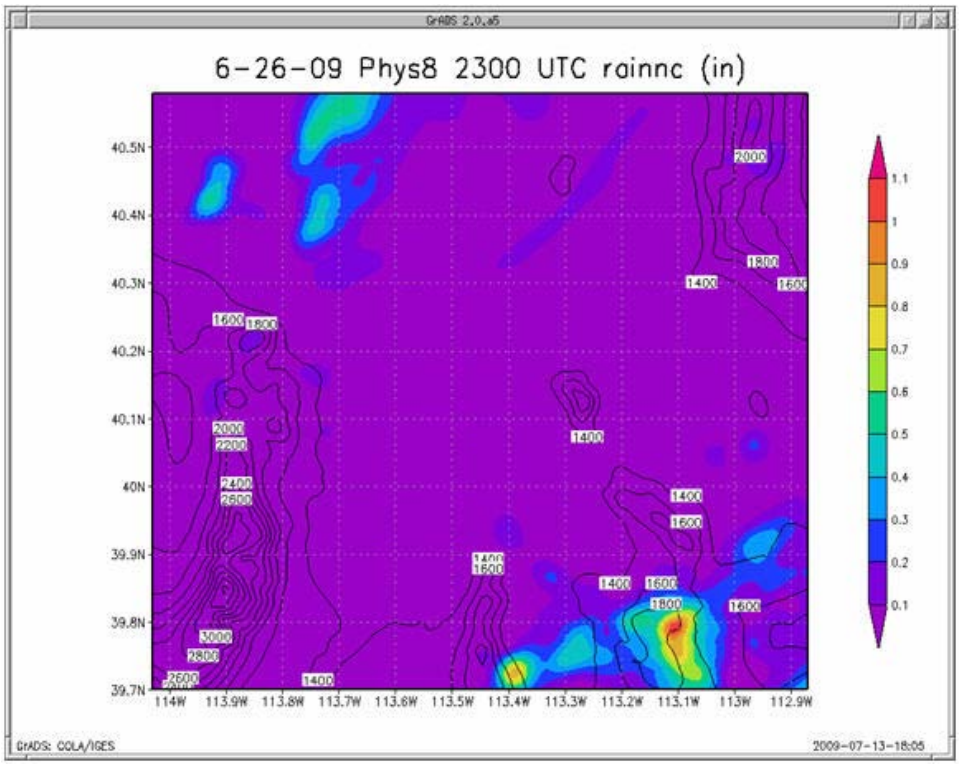

Figure 46. Rainfall totals (mm) for 2300 UTC for the 26 June 2009 model run using the microphysics 8 option.

A few other interesting features did appear on the 26 June model simulations that involve the model interaction between domain 1 and domain 2. As an example, figure 47 shows the wind flow in domain 2 using microphysics option 8. The surface winds are from the south or downvalley by late afternoon as might be expected on a warm summer day. In the northwest corner of the grid, north of 40.3N, there are northwesterly surface winds that appear to be coming from some larger-scale feature. A look at domain 1, the 3-km grid, helps to see this as shown in figure 48.

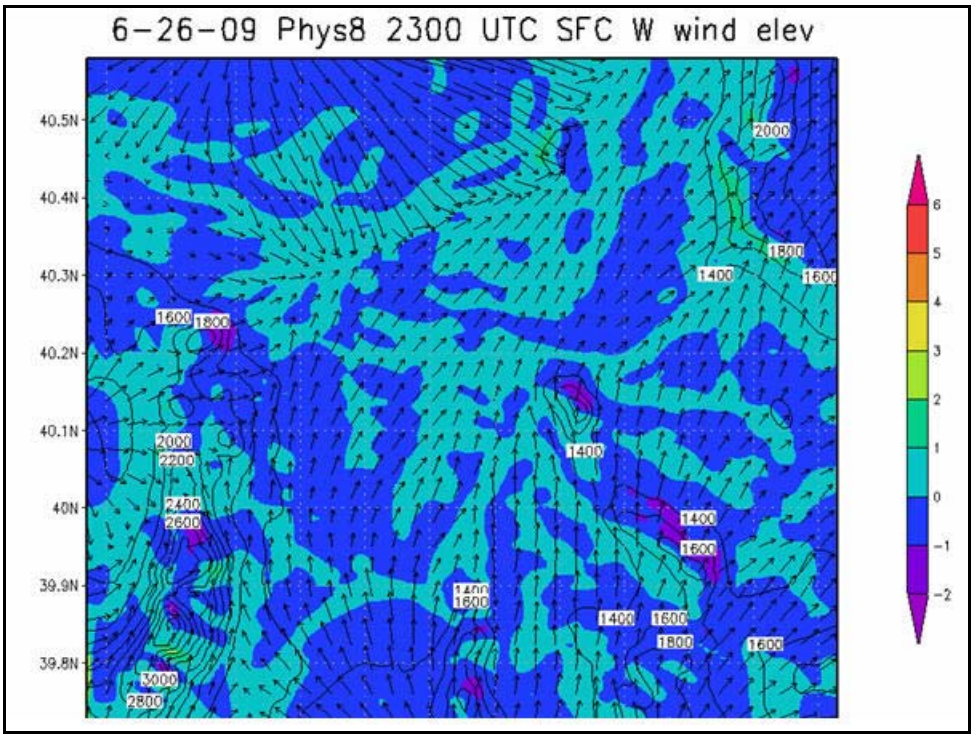

Figure 47. The 26 June 2009 plot of surface winds and vertical motion field (shaded) at surface using microphysics option 8.

Looking at figure 48, the northwest winds appear to be “spilling” over from the larger grid and are being caused by convection on the 3-km grid.

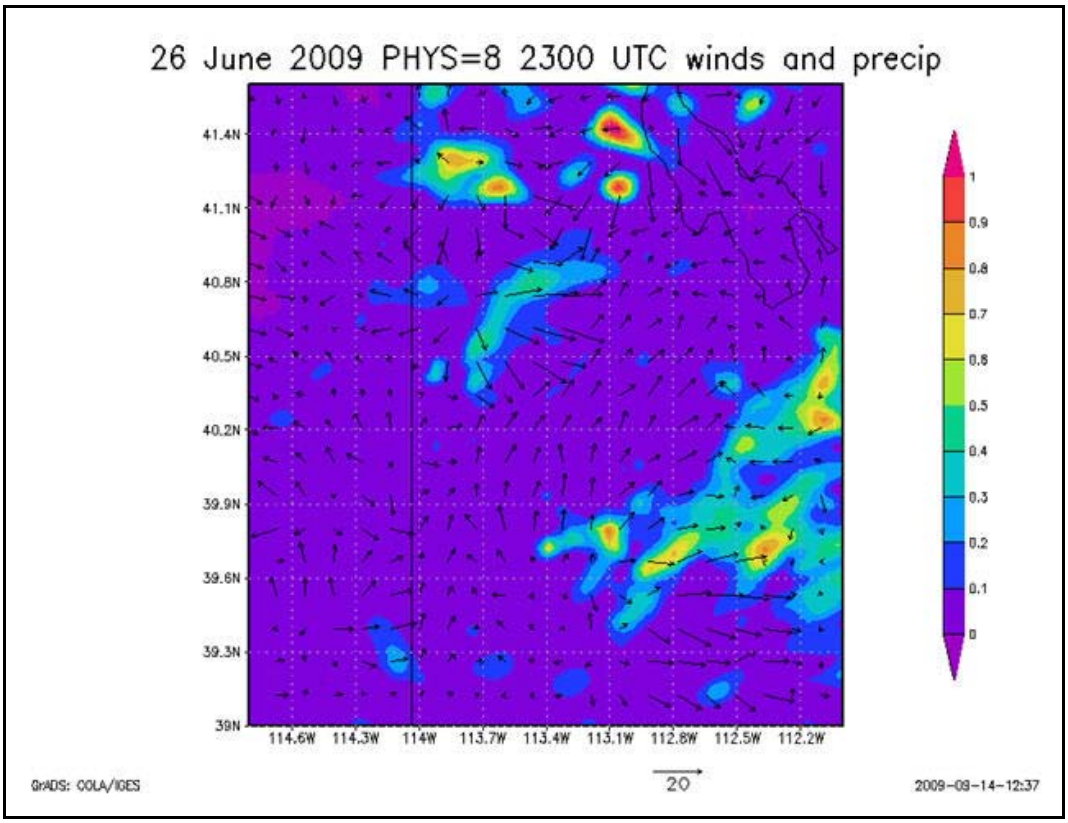

Figure 48. The 26 June 2009 plot of surface winds and accumulated rainfall (mm) at surface using microphysics option 8 for a section of domain 1 (3-km output).

Another model feature is the vertical motion due to the terrain. The model simulations appear to handle the upslope and downslope well with the expected vertical motion fields. While there is no particular way to validate vertical motions, they do make physical sense as seen in figure 49 using the MYJ PBL for domain 2 at 2300 UTC. It can be seen that MYJ scheme produces a south-to-north wind flow down the valley through much of the grid, although there is westerly and some northwesterly wind flow on the western quarter of the domain. Part of this might be driven by convection from the outer domain but it also interacts with the high terrain on the southwest corner of domain 2. The wind component is strong from the west, using the MYJ PBL with rising motions of 3 m/s on the western slopes where upslope is strongest, while sinking motions are strongest at the highest peaks and the downslope side where motions of –2 m/s are forecasted. There are also some areas of weak convergence where the downslope flow interacts with the downvalley winds at the base of the mountain chain. Figure 50 shows this same scenario for the control run. Overall, the two plots show little disparity although the control run shows weaker surface winds and slightly weaker vertical motions.

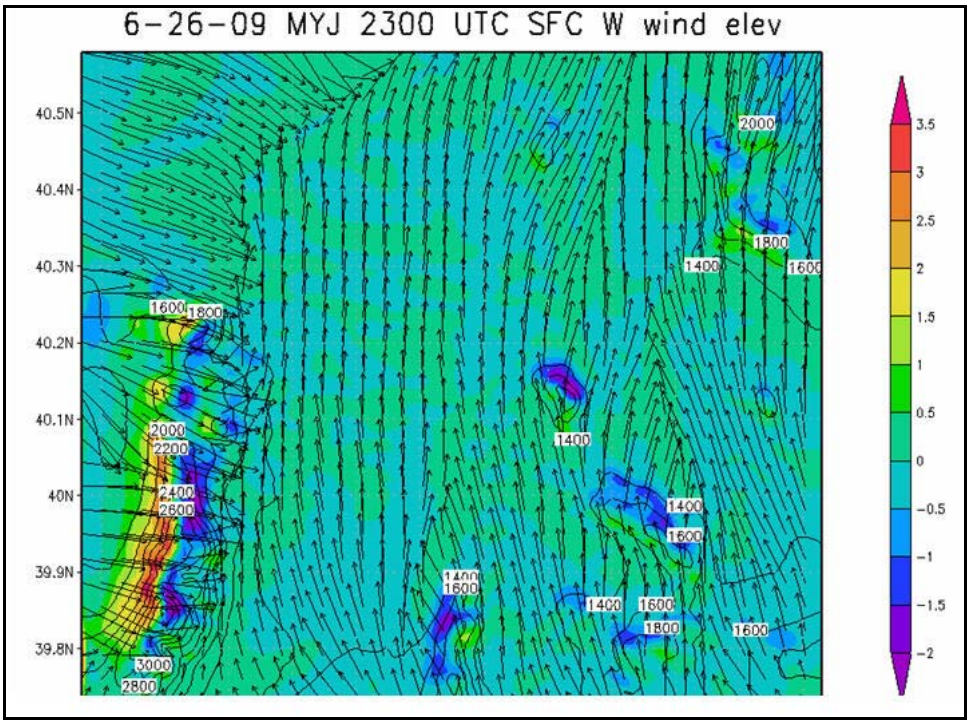

Figure 49. The 26 June 2009 surface winds and vertical motions (shaded) at 2300 UTC using the MYJ PBL.

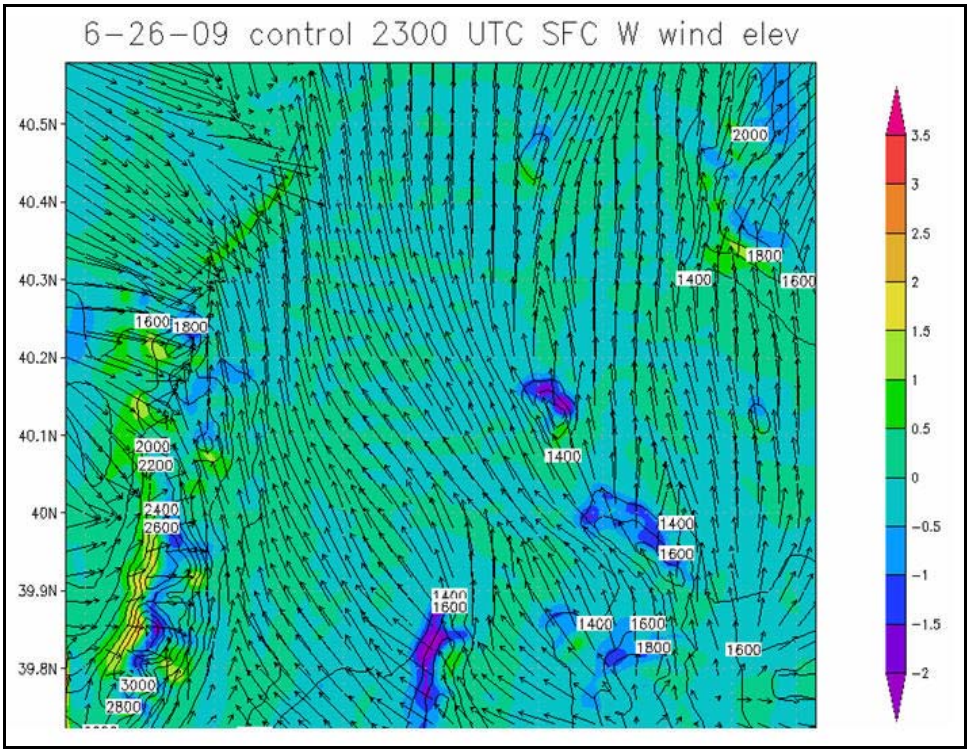

Figure 50. The 26 June 2009 surface winds and vertical motions (shaded) at 2300 UTC using the control run and the YSU PBL.

5. Statistics

Tables 5 and 6 show the surface temperature, dew point temperature, RH, sea level pressure, u-wind component, v-wind component, wind speed, and wind direction for standard surface-level. The results are expressed in ME, MAE, RMSE, and count (CNT), which is the total number of observations for the variable on each day the model was run. Note that the model was run on 8 April 2009, but no surface data was available. The results during the spring months of 2009 show some slight differences between the domains and different parameterizations; however, for the meteorological fields studied, these differences are not significant. There appears to be an improvement in the forecasted temperature field on the 1-km grid compared to the 3-km grid. The root mean square error (RMSE) for the 2-m temperature on the 3-km grid is 2.19 compared to 1.85 on the 1-km grid. Another disparity appears in the pressure field when the RMSE for the larger domain, domain 1 using a 3-km horizontal resolution, is 2.12 compared to 2.96 for the 1-km grid over domain 2. For all other variables (dew point, RH, pressure, and wind) the results were nearly identical or showed only slight differences that were not considered significant.

Table 5. Statistical output for outer nest, domain 1 using the 3-km WRF for nine days during the spring of 2009.

	2 m Temperature (K)				2m DewPoint Temp (K)				2m Rel Humidity (%)				0m MSL Pressure (hPa)			
	ME	MAE	RMSE	CNT	ME	MAE	RMSE	CNT	ME	MAE	RMSE	CNT	ME	MAE	RMSE	CNT
0326	0.29	1.51	1.92	570	0.91	1.59	2.00	553	2.91	8.86	11.50	553	2.15	2.21	2.67	553
0401	-0.39	1.66	2.10	504	2.49	2.90	3.66	488	9.64	13.84	17.80	488	1.31	1.54	1.90	488
0408				0				0				0				0
0415	1.14	1.85	2.36	645	0.13	1.56	2.27	629	-5.07	12.08	16.54	629	0.40	2.09	2.54	629
0421	0.83	2.26	2.85	437	0.29	2.42	2.99	424	-3.62	10.20	13.07	424	-1.53	2.12	2.71	424
0429	-0.13	1.83	2.28	463	1.25	2.26	3.01	446	1.81	8.82	11.43	446	-0.02	1.14	1.46	446
0506	-0.48	2.19	2.68	438	2.38	2.88	3.54	424	6.37	10.94	13.43	424	0.39	1.62	1.97	424
0513	-0.18	1.59	1.99	452	1.94	2.81	3.62	432	4.41	7.24	9.52	432	0.35	1.00	1.30	432
0519	0.43	2.12	2.68	447	-0.01	2.56	3.20	433	-0.82	7.92	10.53	433	-1.72	1.99	2.42	433
0527	0.40	2.26	2.80	448	1.94	2.37	3.05	435	2.27	10.05	12.30	435	-1.12	1.64	2.09	435

													10m Wind Dir (deg)				
	10m U-comp (m/s)				10m V-comp (m/s)				10m Wind Speed (m/s)				ROW_MEAN			AGGR	
	ME	MAE	RMSE	CNT	ME	MAE	RMSE	CNT	ME	MAE	RMSE	CNT	ME	MAE	CNT	ME	CNT
0326	-1.05	2.66	3.41	566	-1.23	3.03	3.89	566	-0.25	2.52	3.08	566	-14.58	14.77	25	-16.77	538
0401	-0.39	2.17	2.85	497	-1.73	2.70	3.85	497	0.13	2.11	2.76	497	-12.59	23.32	25	-19.40	464
0408				0				0				0			0		0
0415	-0.17	2.53	3.13	601	-0.56	3.27	4.31	601	-0.26	2.61	3.32	601	-5.09	32.84	25	-3.78	561
0421	0.29	1.36	1.93	416	-0.84	1.58	2.06	416	-1.14	1.73	2.18	416	2.75	61.96	25	-172.54	315
0429	0.19	1.87	2.43	440	-0.43	1.75	2.31	440	-0.63	1.94	2.44	440	-36.82	47.18	25	-20.03	371
0506	0.24	2.09	2.70	432	-0.69	2.35	3.00	432	-0.65	2.09	2.68	432	-30.61	35.64	25	-15.27	375
0513	-0.44	1.83	2.35	424	0.10	1.97	2.52	424	-0.65	1.90	2.42	424	-9.54	17.16	25	-8.53	382
0519	1.05	2.57	3.37	439	-0.43	2.60	3.40	439	-0.41	2.22	2.85	439	-26.43	31.12	25	-21.11	403
0527	-0.13	1.45	2.02	424	-0.57	1.65	2.14	424	-0.96	1.74	2.19	424	-16.55	49.55	25	-14.50	334

Table 6. Statistical output for inner nest, domain 2, using1-km WRF on nine days during the spring of 2009.

	2 m Temperature (K)				2m DewPoint Temp (K)				2m Rel Humidity (%)				0m MSL Pressure (hPa)			
	ME	MAE	RMSE	CNT	ME	MAE	RMSE	CNT	ME	MAE	RMSE	CNT	ME	MAE	RMSE	CNT
0326	1.51	1.61	1.99	609	-0.62	1.78	2.36	609	-8.77	11.95	15.15	609	2.90	2.93	3.28	484
0401	0.43	1.34	1.76	606	2.48	2.63	3.27	604	6.38	8.64	11.73	604	1.97	2.04	2.42	483
0408				0				0				0				0
0415	1.64	2.02	2.36	602	-2.31	2.85	3.89	598	-16.00	18.00	21.09	598	0.01	1.65	2.04	471
0421	1.24	2.09	2.63	5562	-0.51	2.79	3.29	586	-7.34	11.85	16.05	586	-2.97	2.97	3.16	442
0429	0.47	1.31	1.64	582	0.53	1.68	2.09	586	-0.19	7.07	9.06	586	-0.29	1.78	2.16	462
0506	-1.10	2.05	2.45	584	3.89	3.95	4.55	598	9.91	11.33	13.41	598	-1.56	1.79	2.17	445
0513	0.92	1.45	2.02	605	0.39	2.02	2.62	598	-0.87	3.69	5.29	598	-0.36	1.76	2.10	480
0519	0.55	1.65	2.06	580	-0.21	1.76	2.40	596	-0.55	3.91	5.07	596	-5.47	5.47	5.59	446
0527	0.71	1.81	2.38	591	2.87	3.03	3.50	606	3.89	6.86	8.32	606	-3.56	3.56	3.77	478

	10m U-comp (m/s)				10m V-comp (m/s)				10m Wind Speed (m/s)				10m Wind Dir (deg)				
													ROW_MEAN			AGGR	
	ME	MAE	RMSE	CNT	ME	MAE	RMSE	CNT	ME	MAE	RMSE	CNT	ME	MAE	CNT	ME	CNT
0326	0.55	2.24	2.84	587	-1.21	2.46	3.10	587	1.27	2.38	2.96	587	3.28	9.94	25	2.73	581
0401	1.53	2.30	2.99	584	-1.30	2.64	3.22	584	0.94	2.19	2.78	584	13.35	30.07	25	9.41	569
0408				0				0				0			0		0
0415	-1.54	3.43	4.30	549	1.90	3.72	4.82	549	0.68	2.63	3.30	549	25.83	75.48	25	20.42	528
0421	0.35	1.16	1.46	595	-0.21	1.22	1.53	595	-1.06	1.30	1.59	595	-0.10	33.89	25	93.83	502
0429	-0.44	1.40	1.78	584	0.48	1.63	2.04	584	-0.79	1.34	1.65	584	-30.63	61.11	25	-40.00	517
0506	0.64	2.95	3.68	588	0.18	2.59	3.31	588	0.18	2.21	2.78	588	26.34	62.75	25	7.85	562
0513	-0.15	1.88	2.47	598	0.52	1.86	2.44	598	-0.84	1.80	2.38	598	-17.61	25.58	25	-0.93	574
0519	1.02	2.62	3.26	541	0.29	3.23	4.33	541	-0.05	2.60	3.25	541	-4.64	32.17	25	-12.04	522
0527	-0.16	1.29	1.68	604	0.00	1.26	1.58	604	-0.76	1.22	1.58	604	-5.98	50.58	25	-5.30	531

5.1 Hourly Statistics

The 3-km WRF results for domain 1 hourly surface comparisons are based on all 10 dates, although the April 8 case did not have surface observations available for the domain 2 comparisons. The domain 2 results as well as subsequent comparisons based on model variations include the statistics for each hour from forecast hour 00 to 06, then every three hours from forecast hours 9 to 24. The hourly results can be seen in tables 7 and 8 as well as figures 50–55 where some of the individual parameters are shown during the 24-h forecast period. Overall, the model verification shows some of the trends that might be anticipated. The largest errors in many of the parameters are in the first hours of the model run when the model is still "spinning up" and again at 24 h when model errors start to increase slightly. The only exception to this is the pressure field for some unknown reason where the MAE and RMSE are lower at the 0-h than for the entire first 6-h period.

Table 7. Hourly output for each variable for the outer nest, domain 1, using the 3-km WRF.

	2 m Temperature (K)				2m Dew Point Temp (K)				2m Rel Humidity (%)				0m MSL Pressure (hPa)			
	ME	MAE	RMSE	CNT	ME	MAE	RMSE	CNT	ME	MAE	RMSE	CNT	ME	MAE	RMSE	CNT
0	-0.74	2.37	3.10	233	0.81	2.25	3.09	217	5.61	12.33	15.91	217	-0.37	1.68	2.08	217
1	-0.17	1.82	2.34	192	1.39	2.34	2.99	192	5.26	11.13	13.80	192	-0.42	2.02	2.47	192
2	0.09	1.87	2.38	191	0.93	2.15	2.78	191	2.26	11.32	14.06	191	-0.25	2.00	2.46	191
3	0.45	1.86	2.36	219	0.55	1.90	2.49	208	0.33	11.60	14.88	208	0.05	2.11	2.58	208
4	0.36	1.77	2.30	196	0.68	1.87	2.48	196	1.08	10.96	14.56	196	0.40	2.27	2.77	196
5	0.72	1.94	2.50	192	0.62	1.89	2.52	192	-0.48	11.21	14.81	192	0.07	2.29	2.82	192
6	0.90	2.16	2.70	229	0.72	1.84	2.42	218	-0.45	11.23	14.81	218	-0.26	2.17	2.71	218
7	1.12	1.96	2.50	183	0.73	1.93	2.51	182	-1.24	10.69	14.23	182	-0.24	2.09	2.56	182
8	1.33	1.82	2.38	199	0.93	1.81	2.31	195	-1.38	9.58	12.37	195	-0.05	1.76	2.15	195
9	0.84	1.63	2.13	202	0.56	1.99	2.52	189	-0.85	9.46	12.50	189	0.17	1.36	1.71	189
10	0.59	1.70	2.07	192	0.98	2.03	2.57	188	0.89	9.08	11.97	188	0.53	1.38	1.73	188
11	0.42	1.78	2.26	187	1.26	2.35	2.98	183	0.96	10.05	13.36	183	0.56	1.43	1.85	183
12	0.07	1.78	2.26	217	1.65	2.74	3.44	200	2.52	10.08	13.16	200	0.78	1.45	1.88	200
13	-0.29	1.90	2.32	179	1.65	2.69	3.41	175	3.41	9.40	12.18	175	0.71	1.48	1.88	175
14	-0.30	2.03	2.47	188	1.67	2.70	3.42	186	3.42	9.36	12.04	186	0.66	1.58	2.08	186
15	-0.32	2.14	2.65	208	1.77	2.78	3.63	192	3.20	9.50	12.51	192	0.43	1.70	2.24	192
16	-0.61	2.11	2.65	184	1.75	2.71	3.51	181	3.91	9.08	12.38	181	0.40	1.63	2.02	181
17	-0.48	2.08	2.62	182	1.67	3.04	3.80	181	2.99	10.80	15.21	181	0.26	1.70	2.09	181
18	-0.58	1.97	2.42	218	1.96	2.90	3.81	200	3.63	10.31	14.06	200	0.25	1.50	1.91	200
19	-0.90	1.95	2.41	172	2.12	3.03	3.93	170	5.71	11.47	15.34	170	0.33	1.49	1.89	170
20	-1.00	2.00	2.38	173	2.11	2.94	3.92	173	6.47	12.37	15.30	173	0.40	1.40	1.78	173
21	-0.03	1.67	2.11	206	1.34	2.39	3.10	188	3.26	10.13	13.06	188	-0.32	1.37	1.74	188
22	0.78	1.82	2.33	182	0.76	2.01	2.61	182	-0.76	9.34	12.48	182	-0.74	1.68	2.05	182
23	0.91	1.89	2.35	170	0.61	2.03	2.61	170	-1.15	9.68	12.10	170	-0.72	1.77	2.15	170
24	1.13	2.07	2.62	206	0.42	2.08	2.74	193	-2.44	10.88	13.83	193	-0.35	1.79	2.27	193

													10m Wind Dir (deg)				
	10m U-comp (m/s)				10m V-comp (m/s)				10m Wind Speed (m/s)				ROW_MEAN			AGGR	
	ME	MAE	RMSE	CNT	ME	MAE	RMSE	CNT	ME	MAE	RMSE	CNT	ME	MAE	CNT	ME	CNT
0	0.08	2.29	2.92	230	-0.82	2.64	3.49	230	-0.43	2.27	2.97	230	18.89	37.41	10	-29.56	191
1	-0.05	1.91	2.49	188	-0.84	2.18	2.85	188	-0.98	2.17	2.75	188	-26.32	30.43	10	-37.36	160
2	0.31	2.22	2.92	190	-1.22	2.46	3.12	190	-0.60	2.44	3.09	190	-40.35	40.35	10	-51.30	163
3	0.14	2.12	2.84	216	-0.90	2.37	3.22	216	-0.32	2.27	3.00	216	-25.63	29.97	10	-30.94	191
4	-0.08	2.29	3.11	195	-0.95	2.75	3.53	195	-0.71	2.73	3.40	195	-35.53	41.01	10	-39.96	166
5	0.17	2.16	2.90	190	-1.02	2.53	3.30	190	-0.66	2.32	2.91	190	-45.66	49.81	10	-40.76	161
6	0.23	2.22	2.93	224	-1.01	2.72	3.60	224	-0.98	2.53	3.23	224	-33.76	44.37	10	-43.64	199
7	0.43	2.19	2.85	179	-1.14	2.70	3.73	179	-1.18	2.42	3.00	179	-37.21	57.39	10	-45.13	158
8	0.48	2.16	2.84	196	-0.97	2.59	3.84	196	-0.54	2.26	3.00	196	-48.75	48.75	10	-35.36	169
9	0.69	2.04	2.77	198	-1.06	2.41	3.46	198	-0.15	2.01	2.62	198	-52.09	54.43	10	-42.36	170
10	0.09	2.10	2.79	182	-1.27	2.37	3.30	182	-0.49	1.99	2.61	182	-25.56	49.56	10	-46.59	159
11	0.47	2.29	3.17	162	-1.16	2.48	3.56	162	-0.50	2.18	2.85	162	-2.76	25.76	10	-33.39	146
12	-0.39	2.51	3.16	204	-1.05	2.68	3.70	204	-1.13	2.35	2.99	204	2.23	17.28	10	-34.76	192
13	-0.66	2.42	3.14	167	-1.07	2.78	3.57	167	-1.01	2.37	3.01	167	13.96	29.12	10	-26.83	153
14	-0.82	2.45	3.19	178	-0.75	2.69	3.67	178	-0.99	2.33	2.84	178	-7.30	29.87	10	-19.76	173
15	-0.57	2.73	3.56	193	-0.78	2.87	3.74	193	-0.78	2.24	2.91	193	-7.03	16.47	10	-16.76	188
16	0.15	2.50	3.31	173	-0.74	2.69	3.49	173	-0.24	2.18	2.67	173	-7.11	13.41	10	-14.62	167
17	0.26	2.62	3.45	169	0.03	2.87	3.93	169	-0.50	1.92	2.40	169	2.00	15.51	10	1.92	161
18	0.38	2.45	3.20	210	-0.58	2.45	3.42	210	0.03	2.06	2.60	210	-14.85	14.91	10	-12.65	197
19	-0.07	1.85	2.45	168	-0.21	2.42	3.40	168	-0.28	1.89	2.38	168	0.96	21.02	10	-6.59	156
20	-0.16	2.04	2.82	168	-0.50	2.30	3.23	168	0.12	1.98	2.73	168	-21.76	24.81	10	-21.90	149
21	-0.48	1.97	2.63	203	-0.54	2.01	2.65	203	-0.26	1.88	2.38	203	-25.61	28.75	10	-30.37	180
22	0.33	2.16	2.75	177	-0.93	2.19	2.95	177	0.07	2.15	2.75	177	6.91	52.15	10	-55.09	153
23	0.32	2.00	2.79	169	-1.00	2.27	2.95	169	-0.01	2.13	2.74	169	-14.15	41.41	10	-52.37	148
24	0.46	2.01	2.62	203	-1.05	2.11	2.91	203	0.16	2.06	2.62	203	-17.65	42.78	10	-74.27	162

Table 8. Hourly output for each variable for the inner nest, domain 2, using the 1-km WRF output.

	2 m Temperature (K)				2m DewPoint Temp (K)				2m Rel Humidity (%)				0m MSL Pressure (hPa)			
	ME	MAE	RMSE	CNT	ME	MAE	RMSE	CNT	ME	MAE	RMSE	CNT	ME	MAE	RMSE	CNT
0	0.42	2.43	3.08	210	0.38	3.21	4.00	214	0.52	13.77	17.46	214	-1.25	2.28	2.90	167
1	0.17	1.73	2.15	209	0.41	2.60	3.32	214	0.67	12.66	15.39	214	-1.18	2.62	3.25	165
2	0.75	1.60	1.99	207	0.28	2.49	3.01	216	-1.40	10.71	13.09	216	-0.55	2.51	3.04	167
3	1.16	1.82	2.33	206	1.00	2.39	2.94	216	-1.22	11.11	14.12	216	0.04	2.66	3.02	165
4	1.12	1.78	2.35	207	0.99	2.34	2.90	215	-1.04	11.49	14.47	215	0.52	2.98	3.34	168
5	1.49	1.86	2.50	205	0.86	2.18	2.84	212	-2.68	11.60	15.04	212	0.37	2.80	3.19	166
6	1.62	2.00	2.63	201	0.62	2.04	2.56	212	-4.22	10.73	13.96	212	0.43	2.67	3.06	165
7																
8																
9	0.49	1.40	1.75	217	0.14	2.00	2.45	218	-1.95	8.33	11.19	218	-0.10	2.50	3.02	171
10																
11																
12	0.35	1.75	2.21	221	-0.10	2.51	3.23	221	-3.26	8.83	13.13	221	-0.99	2.26	2.76	173
13																
14																
15	0.04	1.45	1.82	222	0.14	2.57	3.48	222	-1.95	6.99	11.54	222	-1.88	2.51	3.00	170
16																
17																
18	0.09	1.52	1.87	216	0.84	2.94	3.54	213	-0.36	7.33	10.45	213	-2.76	3.34	3.88	167
19																
20																
21	1.09	1.54	1.85	203	1.92	2.77	3.55	198	0.18	8.79	11.32	198	-1.57	2.72	3.23	157
22																
23																
24	1.96	2.25	2.78	210	1.53	2.69	3.43	210	-2.46	9.52	12.10	210	-0.70	2.63	3.12	166

													10m Wind Dir (deg)				
	10m U-comp (m/s)				10m V-comp (m/s)				10m Wind Speed (m/s)				ROW_MEAN			AGGR	
	ME	MAE	RMSE	CNT	ME	MAE	RMSE	CNT	ME	MAE	RMSE	CNT	ME	MAE	CNT	ME	CNT
0	1.33	2.41	3.16	202	1.19	3.08	3.91	202	-1.67	2.28	2.95	202	10.92	37.59	9	55.49	189
1	0.79	2.47	3.18	206	0.03	2.38	3.10	206	-0.22	2.41	3.06	206	25.24	36.00	9	18.32	193
2	1.10	2.45	3.20	201	0.60	2.19	2.86	201	0.23	2.24	2.86	201	-16.10	55.16	9	30.69	185
3	1.26	3.06	4.02	205	0.27	2.15	2.82	205	-0.01	2.15	2.79	205	-0.09	52.26	9	24.40	193
4	1.18	2.29	3.07	206	0.68	2.59	3.63	206	0.17	2.34	3.04	206	49.32	72.67	9	28.54	185
5	1.04	2.06	2.65	212	0.06	2.21	2.89	212	-0.18	2.03	2.55	212	-4.67	47.03	9	19.25	183
6	0.78	1.98	2.60	209	-0.40	2.24	2.88	209	-0.08	2.09	2.60	209	48.24	57.23	9	16.71	189
7																	
8																	
9	0.49	1.75	2.34	214	-0.72	1.92	2.69	214	-0.08	1.65	2.33	214	-5.08	43.01	9	11.83	180
10																	
11																	
12	-0.03	1.73	2.24	212	-0.18	1.86	2.33	212	-0.25	1.81	2.29	212	-17.97	21.00	9	-10.15	205
13																	
14																	
15	-0.65	2.38	3.22	214	1.24	2.60	3.47	214	0.05	2.20	2.91	214	-2.99	44.23	9	18.06	210
16																	
17																	
18	-0.27	2.47	3.41	204	1.50	3.11	4.71	204	0.06	1.92	2.51	204	11.02	43.89	9	7.69	203
19																	
20																	
21	0.34	2.10	2.77	203	-0.76	2.03	2.66	203	0.80	1.85	2.39	203	1.75	48.03	9	15.02	190
22																	
23																	
24	-0.29	2.17	2.86	213	-0.97	2.09	2.62	213	-0.01	1.91	2.40	213	-14.06	45.54	9	-53.23	193

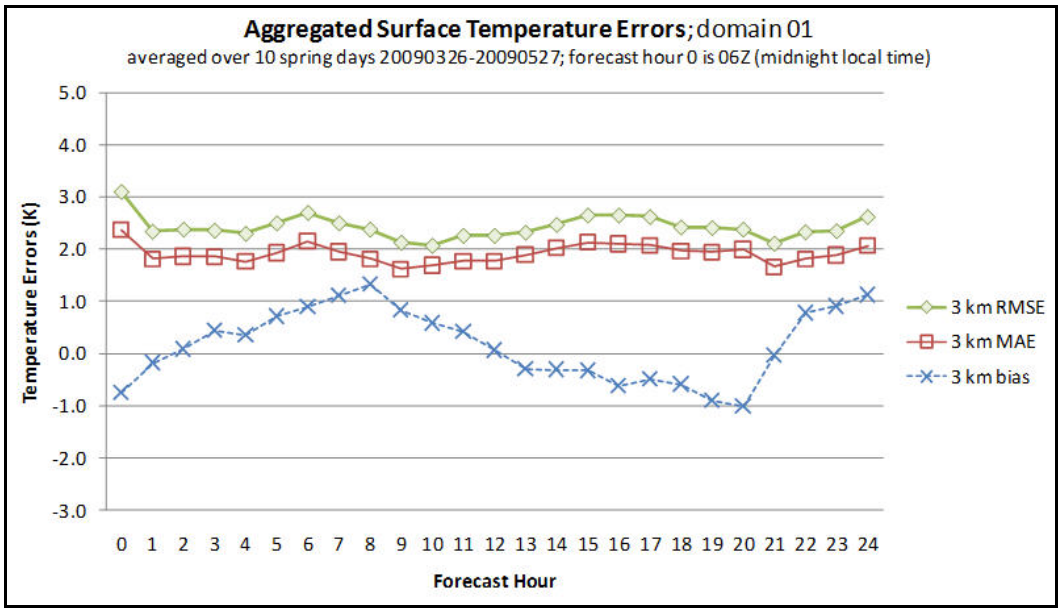

Figure 51. Surface temperature error for outer nest (domain 1) over the 24-h forecast period.

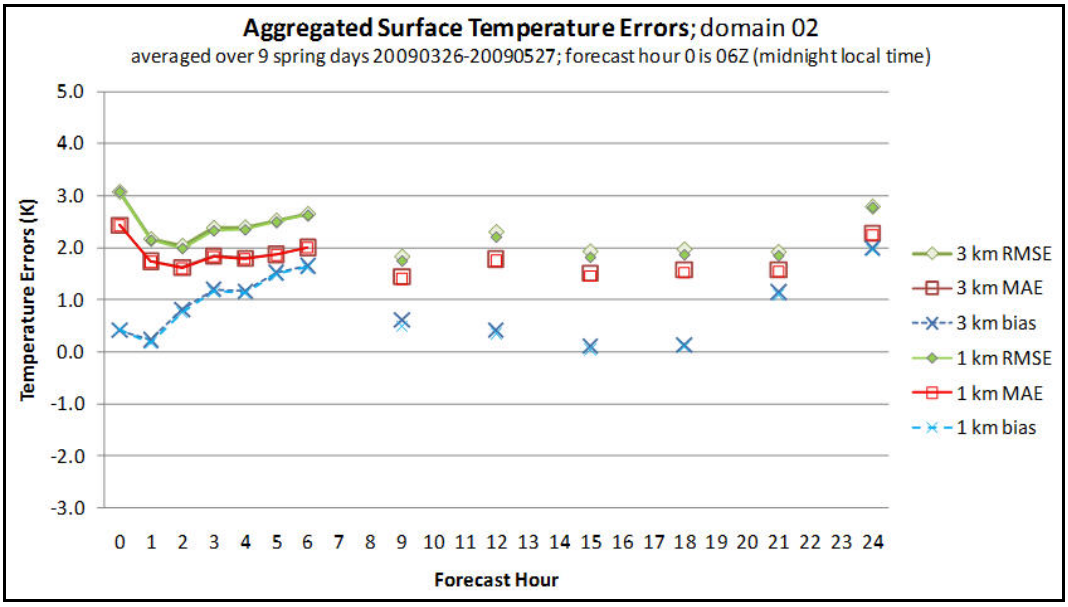

Figure 52. Surface temperature error for inner nest (domain 2) over the 24-h forecast period.

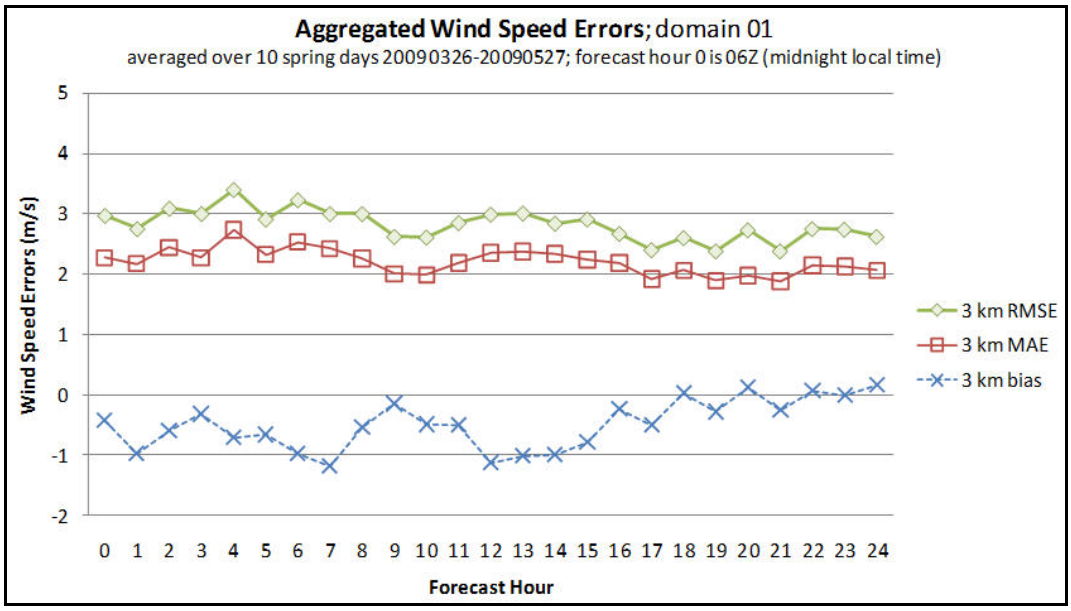

Figure 53. Surface windspeed error for outer nest (domain 1) over the 24-h forecast period.

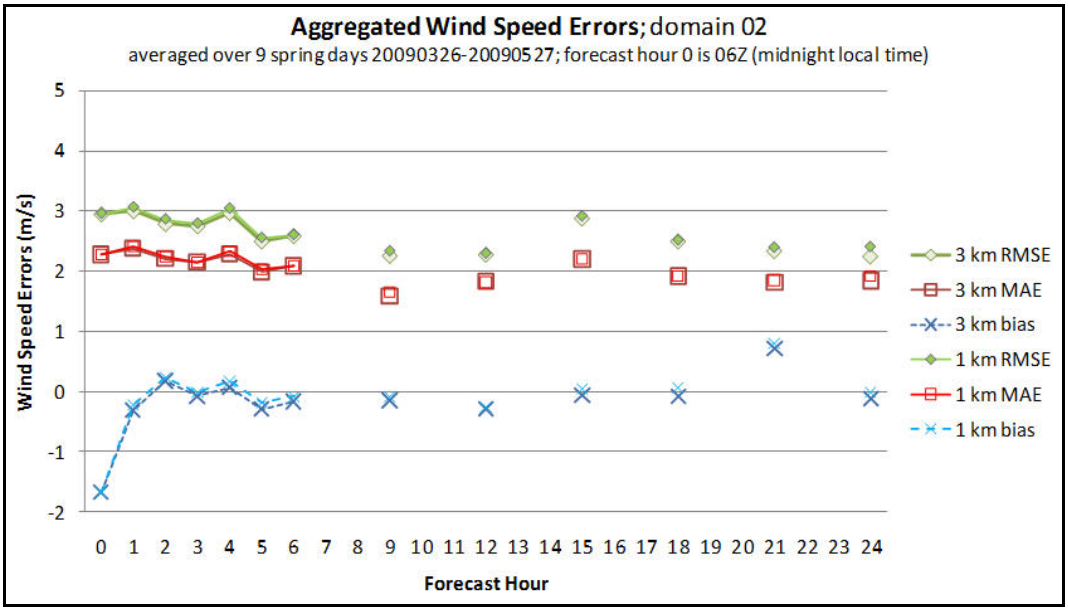

Figure 54. Surface windspeed error for inner nest (domain 2) over the 24-h forecast period.

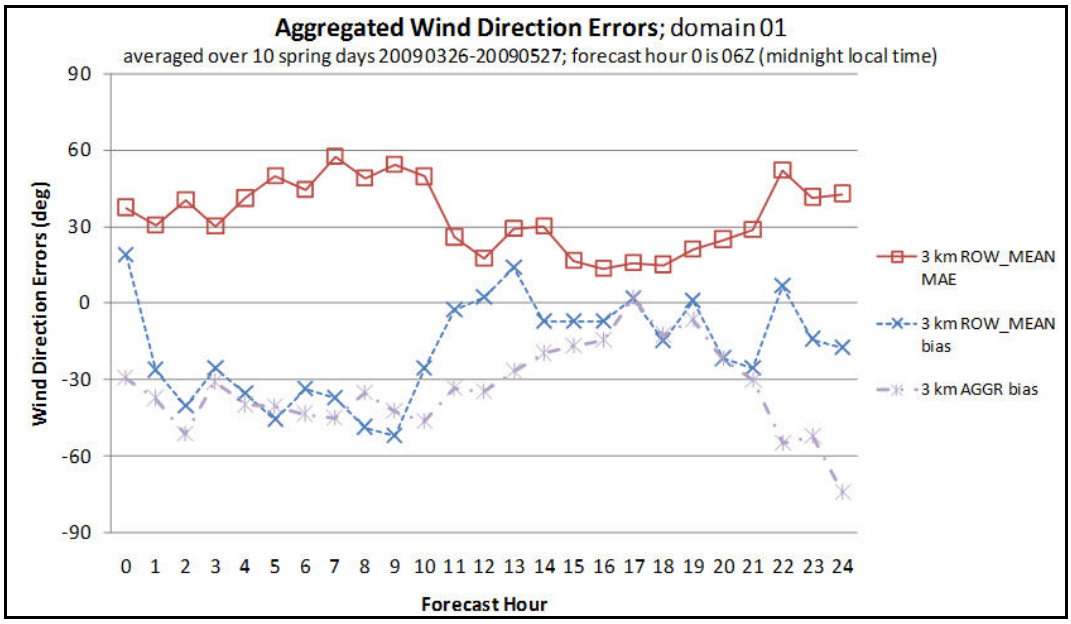

Figure 55. Wind direction error for outer domain (domain 1) for the 24-h forecast period.

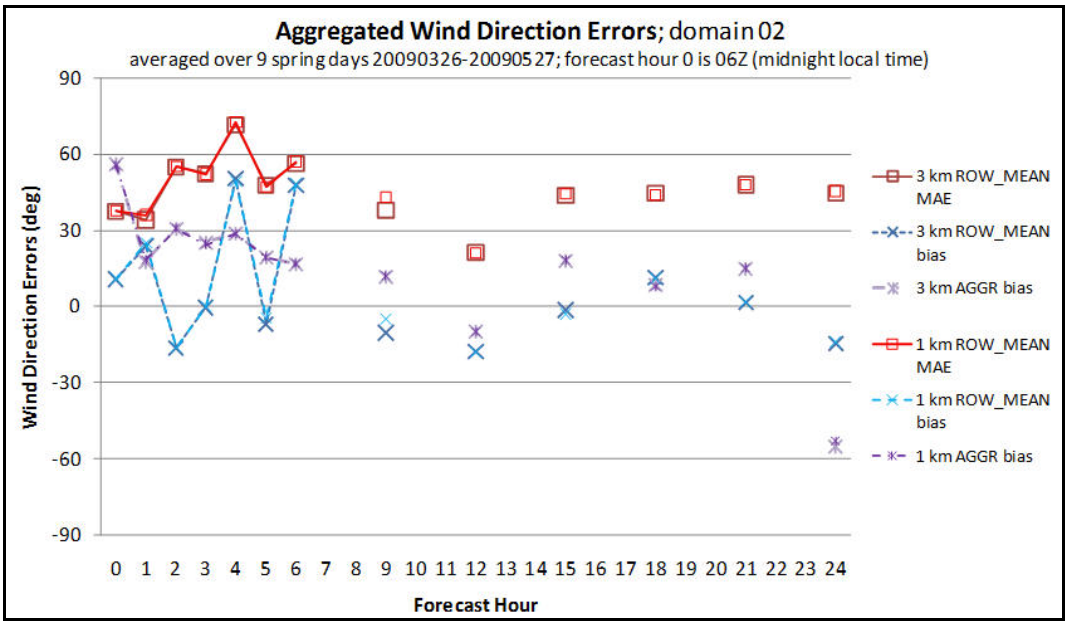

Figure 56. Wind direction error for inner domain (domain 2) for the 24-h forecast period.

5.2 Results by Model Parameterization

Tables 9 and 10 display the model results for the 26 March case for both domain 1 and domain 2 for the different model simulations and parameterizations. For this one case, there is little difference in the model statistics from model to model. The wind speed and wind directions appear more accurate on domain 2 while the temperature and surface moisture fields display less error on domain 1 than domain 2. However, since this is one case, these results are not significant. Again, the most intriguing finding in this case is the uniformity in the output from

model simulation to model simulation. It should be noted that this is not the case with all the meteorological parameters and much of this report has shown the wide disparity in the upper-air moisture, short-wave radiation, and precipitation fields for all the cases.

Table 9. The 3-km WRF (domain 1); model variation on 26 March 2009.

	2 m Temperature (K)				2m DewPoint Temp (K)				2m Rel Humidity (%)				0m MSL Pressure (hPa)			
	ME	MAE	RMSE	CNT	ME	MAE	RMSE	CNT	ME	MAE	RMSE	CNT	ME	MAE	RMSE	CNT
Control	0.29	1.51	1.92	570	0.91	1.59	2.00	553	2.91	8.86	11.50	553	2.15	2.21	2.67	553
3 sec	0.20	1.47	1.90	570	1.11	1.69	2.13	553	4.40	9.31	11.92	553	2.18	2.24	2.71	553
40 lev	0.37	1.52	1.95	570	0.83	1.55	1.96	553	2.05	8.77	11.33	553	2.32	2.37	2.84	553
80 lev	0.26	1.51	1.92	570	0.95	1.61	2.03	553	3.31	8.99	11.68	553	2.06	2.13	2.58	553
phys 2	0.32	1.55	1.96	570	0.92	1.61	2.05	553	2.80	8.83	11.48	553	2.01	2.12	2.60	553
phys 8	0.08	1.47	1.90	570	1.14	1.63	2.05	553	4.89	9.23	11.86	553	2.40	2.44	2.87	553
bl myj	0.38	1.47	1.90	570	0.80	1.71	2.16	553	1.91	9.54	12.11	553	2.27	2.32	2.77	553

	10m U-comp (m/s)				10m V-comp (m/s)				10m Wind Speed (m/s)				10m Wind Dir (deg) ROW_MEAN			AGGR	
	ME	MAE	RMSE	CNT	ME	MAE	RMSE	CNT	ME	MAE	RMSE	CNT	ME	MAE	CNT	ME	CNT
Control	-1.05	2.66	3.41	566	-1.23	3.03	3.89	566	-0.25	2.52	3.08	566	-14.58	14.77	25	-16.77	538
3 sec	-1.10	2.72	3.47	566	-1.16	2.95	3.79	566	-0.34	2.46	3.04	566	-14.92	14.98	25	-17.05	553
40 lev	-1.12	2.71	3.45	566	-1.22	2.98	3.82	566	-0.31	2.52	3.07	566	-15.27	15.36	25	-17.46	553
80 lev	-1.05	2.66	3.40	566	-1.20	3.01	3.86	566	-0.25	2.49	3.04	566	-14.24	14.41	25	-16.61	553
phys 2	-1.07	2.72	3.50	566	-1.21	3.06	3.92	566	-0.22	2.59	3.20	566	-14.46	14.67	25	-16.87	553
phys 8	-1.05	2.62	3.31	566	-1.07	2.98	3.85	566	-0.39	2.50	3.09	566	-14.30	14.39	25	-16.17	553
bl myj	-0.84	2.56	3.29	566	-1.45	3.25	4.16	566	0.24	2.53	3.15	566	-11.87	12.38	25	-15.10	553

Table 10. The 1-km WRF (domain 2); model variation on 26 March 2009.

	2 m Temperature (K)				2m DewPoint Temp (K)				2m Rel Humidity (%)				0m MSL Pressure (hPa)			
	ME	MAE	RMSE	CNT	ME	MAE	RMSE	CNT	ME	MAE	RMSE	CNT	ME	MAE	RMSE	CNT
Control	1.51	1.61	1.99	609	-0.62	1.78	2.36	609	-8.77	11.95	15.15	609	2.90	2.93	3.28	484
3 sec	1.51	1.62	1.99	609	-0.58	1.80	2.38	609	-8.42	11.72	14.98	609	2.86	2.89	3.22	553
40 lev	1.54	1.64	2.03	609	-0.72	1.87	2.46	609	-9.33	12.55	15.77	609	3.09	3.11	3.44	484
80 lev	1.51	1.61	1.98	609	-0.54	1.77	2.34	609	-8.34	11.68	14.89	609	2.82	2.86	3.21	484
phys 2	1.58	1.65	2.01	609	-0.68	1.73	2.34	609	-9.35	11.50	14.74	609	2.74	2.78	3.13	484
phys 8	1.23	1.43	1.85	609	-0.09	1.79	2.28	609	-4.94	11.15	14.33	609	3.22	3.25	3.62	484
bl myj	1.42	1.54	1.98	609	-0.22	1.76	2.34	609	-6.66	11.11	14.23	609	3.00	3.03	3.40	484

	10m U-comp (m/s)				10m V-comp (m/s)				10m Wind Speed (m/s)				10m Wind Dir (deg) ROW_MEAN			AGGR	
	ME	MAE	RMSE	CNT	ME	MAE	RMSE	CNT	ME	MAE	RMSE	CNT	ME	MAE	CNT	ME	CNT
Control	0.55	2.24	2.84	587	-1.21	2.46	3.10	587	1.27	2.38	2.96	587	3.28	9.94	25	2.73	581
3 sec	0.60	2.23	2.82	587	-1.14	2.45	3.08	587	1.21	2.35	2.92	587	3.63	10.12	25	3.12	581
40 lev	0.51	2.16	2.77	587	-1.19	2.46	3.09	587	1.24	2.37	2.94	587	2.73	9.67	25	2.45	581
80 lev	0.58	2.25	2.84	587	-1.19	2.48	3.11	587	1.26	2.38	2.97	587	3.63	9.86	25	2.92	581
phys 2	0.46	2.17	2.73	587	-1.24	2.58	3.20	587	1.26	2.45	3.01	587	3.08	10.22	25	2.06	581
phys 8	1.02	2.29	2.86	587	-0.95	2.37	3.02	587	1.12	2.27	2.86	587	6.33	11.59	25	6.12	581
bl myj	0.84	2.30	2.95	587	-1.39	2.66	3.33	587	1.69	2.62	3.25	587	5.55	8.55	25	4.36	581

There are modest differences between the 3-km outer domain and the 1-km inner domain in most parameters. The temperature fields appear to more accurate using 1-km output in domain 2 (inner nest). While there is variation on individual days as to which grid provided more accurate results, the overall differences over the nine days tested show little significant scatter. Most of the variables show the largest errors at the initial time period, except the surface pressure for some unknown reason. The trend is for higher errors as the model spins up in the first few hours of the model simulation.

6. Discussion

Three different microphysics schemes were used in the model simulations in this project. They are:

1. Lin's scheme (mp_physics=2) which is a 6-class scheme that includes graupel, ice sedimentation, and time split fall terms (Lin et al., 1983).
2. WSM (WRF single-moment microphysics scheme) 5-class scheme (mp_physics=4). This includes ice, supercooled water, snow melt, ice sedimentation, and time-split fall terms (Hong et al., 2004).
3. Thompson's scheme (mp_physics=8). This is an upgrade from Thompson's 2004 scheme and include 6-classes including grapuel and time-split fall terms. The routine also included ice-number concentration which makes it a double-moment scheme for ice (Thompson et al., 2006).

In the WRF the microphysics is integrated outside the 3rd order Runge-Kutta time integration scheme so that the values of saturation remain correct. The mixing ratios of cloud water, cloud ice, non-precipitation water, rain, snow, and graupel are predicted at each grid point based on advection, production, and fallout (Lin et al., 1983). WRF modelers recommend that for less than 10-km horizontal resolutions that the microphysics schemes include a mixed-phase process. All three methods tested do. These routines are also considered single-moment schemes, meaning that only the total mixing ratio is predicted. One of the main findings in the research is the importance of the cloud ice contribution to the microphysics scheme and resulting precipitation. Thompson, with his new snow treatment, reduces the ice supersaturation at high altitudes (low temperatures) and within deep glaciated clouds but enhances supercooled liquid water in shallow, relatively warm clouds. This aspect combined with rain size distribution intended to mimic both classical and non-classical precipitation-formation mechanisms seems to improve forecasts in freezing drizzle and icing. While Thompson's scheme is a double-moment scheme in cloud ice, it should be noted that double-moment routines are computationally costly. A study by Wang et al. (2009), using a 2-D thunderstorm simulation at 250-m resolution, illustrated the wide discrepancy of the ice-phase microphysics. At a 4-km resolution they found

that the ice-phase contributes most to the wide discrepancy between the model output and observations. Additionally, work done at NCAR (refer to NCAR Research Applications Laboratory | RAL. Cloud Microphysics Page in the references) mentions that ice initiation is not well understood because it's difficult to observe and measure. The interaction between the microphysics and other physical processes is very complex and the amount and size of cloud water and ice water greatly influence the radiation schemes, which will influence the heating, cooling, and moisture processes at the surface.

Much of the work in this study agrees with the findings in other studies. There are vast differences in the mixing ratios of water vapor, ice, snow, and rain water with each microphysics routine studied. Additionally, it appears that the ice mixing ratio greatly influences precipitation even in convective, warm-season cases. While the sample size is limited to four cases in this study, it follows some studies that indicate that microphysics 2, Lin's scheme, tends to overforecast precipitation, such as the 26 March case. However, on 26 June, a convective case, Lin's scheme does not produce as much precipitation as some of the others. Additionally, the amount and location of the convective precipitation differ greatly at 2300 UTC in each case. It follows in the 26 June case that Lin's scheme produces the least amount of qice and produces the least amount of precipitation. It also appears that qice varies in amount and height in all three schemes. While it is impossible to make the conclusion that qice is the essential variable for precipitation total, it does appear to play a key role.

The parameterization of turbulence in the PBL and in the free atmosphere represents a nonsingular implementation of the Mellor-Yamada Level 2.5 turbulence closure model through the full range of atmospheric turbulent regimes (Chiao, 2006). Turbulent Kinetic Energy (TKE) production is nonsingular in the case of growing turbulence. In the stable range, the upper limit is derived from the requirement that the ratio of the variance of the vertical velocity deviation and TKE cannot be smaller than that corresponding to the regime of vanishing turbulence. The MRF scheme (Hong and Pan, 1996) uses enhanced vertical flux coefficients in the PBL and height is determined from a critical bulk RI. It handles vertical diffusion with an implicit local scheme and is based on local RI in the free atmosphere. The YSU scheme is a modification of the MRF scheme to reduce nonlocal mixing and to include explicit entrainment fluxes of heat, moisture, and momentum, counter-gradient transport of momentum and different specification of the PBL height.

A study in the difference in the PBL (Gallus et al., 2005) in convective cases found that the MYJ scheme was too cool, moist, and too shallow while the YSU scheme proved to be too warm and dry with the height of the PBL too deep. Differences in the PBL were more pronounced in clear conditions, which show a strong relationship to radiative heating. Additionally, these trends were more noticeable at 0000 UTC rather than 1200 UTC, which hints at the relationship to daytime heating. In the convective case in this study, the 26 June 2009 case, the temperature field trends were opposite of the Gallus et al. (2005) study, with the YSU being cooler and MYJ scheme warmer at 2300 UTC; although, there was little difference in the temperature field noted

at 1100 UTC when convection was ongoing on the western edge of domain 2. The MYJ did seem more rigid in the upvalley and downvalley flow, while the YSU scheme did seem to respond slightly better to terrain differences in the valley or basin locations. Additionally, the YSU scheme showed warmer temperature and possibly more response to the downslope winds. At 1100 UTC, another interesting feature was the nature of the convection with both schemes using microphysics 4. The YSU produced more linear convection as displayed in figure 57 while the MYJ scheme produced more cellular convection as shown in figure 58. More investigation will be needed to fully understand how and why the PBL conditions change the wind flow and precipitation totals, given that both are using the identical microphysics package. A much more detailed statistical study will be needed to learn if one PBL is more effective than another and in what conditions.

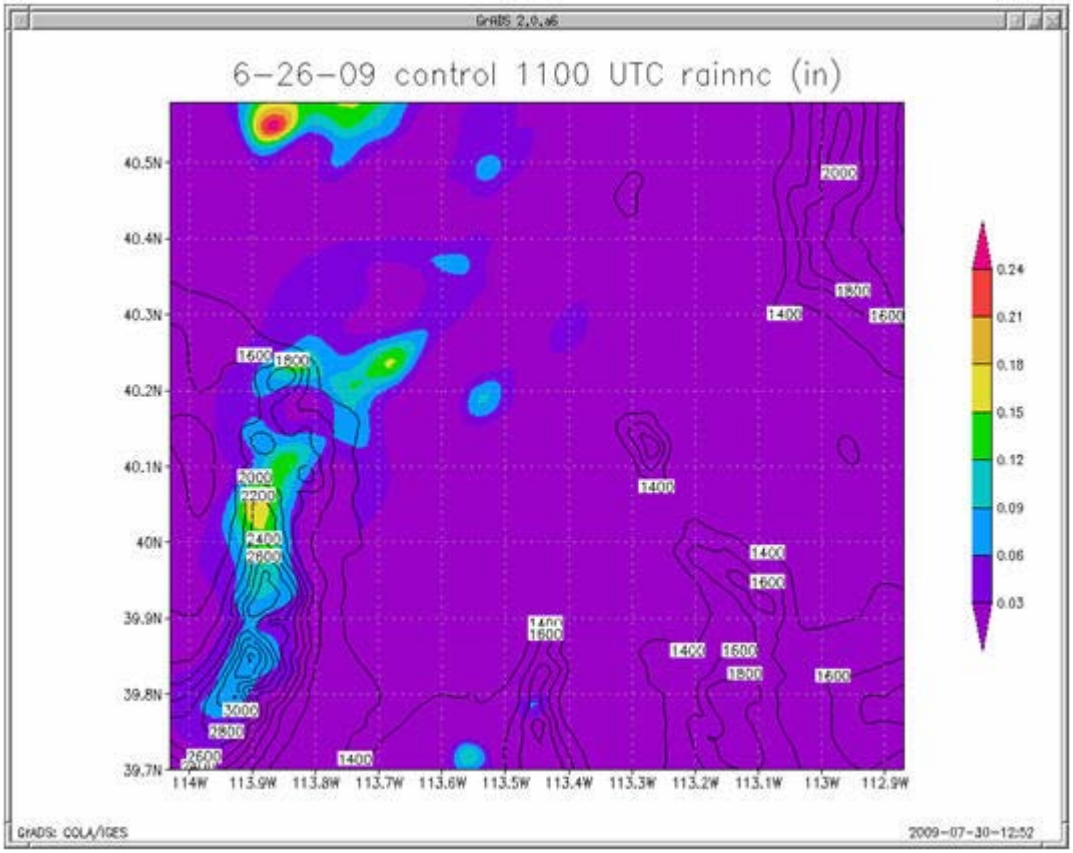

Figure 57. YSU convection at 1100 UTC, 26 June 2009.

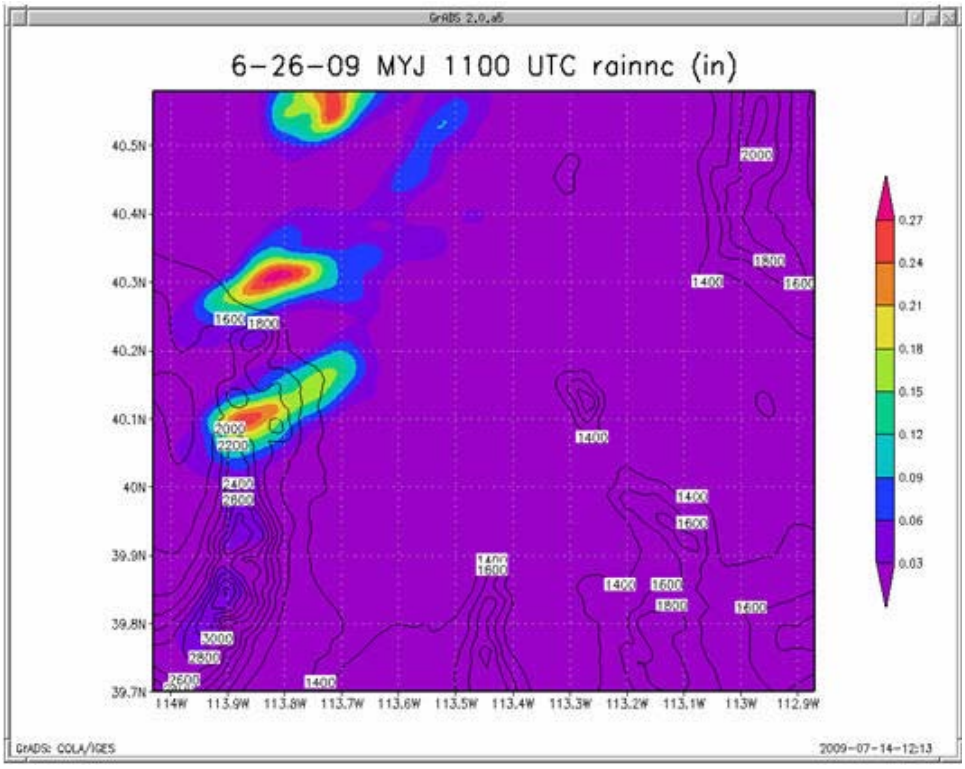

Figure 58. MYJ convection at 1100 UTC, 26 June 2009.

Changing the time step from 9 to 3 sec did not provide obvious advantages or disadvantages. An older study by Mei et al. (2001) with the MM5 found that precipitation amounts seem most sensitive to changes in the time step. They found the precipitation amounts can change by 50% when the time step is reduced from 225 to 150 sec. Their study noted that the temperature field and 850-hPa vertical motion field did not change much as time steps are reduced. In this current work with the WRF, the 26 June 2009 case over DPG found a similar trend. Using the control run (9-sec time step) over domain 2 the maximum 24-h precipitation was 11.4 mm; however, a model run using a 3-sec time step on the same domain produced a maximum precipitation total of 27.9 mm.

The final area of model comparison here was using 40 and 80 levels in different simulations. Once again, statistical evaluation needs to be completed with far more cases, but it does appear that the 80-level simulation did produce more detailed surface wind features with sharper divergence around the terrain features and stronger downslope winds. Additionally, there is some evidence that it provides warmer temperatures at the base of the mountain ranges experiencing downslope flow.

7. Conclusions

It should be noted, any conclusions in this study should be taken with caution at this time. High resolution models are extremely difficult to verify due to data scarcity and physics limitations. Model variations and model physics have not been fully studied with the WRF or any mesoscale model and much additional work still needs to be completed. Future work will focus on more detailed verification of the model microphysics, model resolution, and PBLs. This will require more simulations in data-rich regions and in unique meteorological conditions to provide more balance in the statistical evaluation. Additionally, work was done with upper-air data but is not discussed in this report due to the volume of those data. Future reports will include some of those findings since the upper-air features also answer questions about model output. Overall, this work has provided a vital foundation to build on. Discoveries were made in many areas, but many questions still need additional work and plans are being made to enhance this effort with more detailed evaluation.

8. References

Chiao, S. Performance of planetary boundary layer schemes in the WRF model. *Proceedings of the 25th Army Science Conference*, Orlando, FL, November 27–30, 2006.

Dumais, R. E.; Passner, J. E.; Flanigan, R.; Sauter, B.; Kirby, S. High Resolution WRF-ARW Studies at the U.S. Army Research Laboratory for use in Short-Range Forecast Applications. P2.4. *23rd Conference on Weather Analysis and Forecasting/19th Conference on numerical Weather Prediction*. Omaha, NE, June 1–5, 2009.

Gallus, W.A.; Jankov, I.; Aligo, E. Impacts of Grid Spacing and Physical Parameterizations on WRF Simulations of Convective System Rainfall and Morphology. Summer 2005. http://www.dtcenter.org/visitors/reports_05/gallus.pdf (accessed October 22, 2009).

Hong, S. Y.; Dudhia, J.; Chen, S. H. A Revised Approach to Ice Microphysical Processes for the Bulk Parameterization of Clouds and Precipitation. *Mon. Wea. Rev.* **2004**, *132*, (1), 103–120.

Hong, S. Y; Pan, H. L. Nonlocal Boundary Layer Vertical Diffusion in a Medium Range-Forecast Model. *Mon. Wea. Rev.* **1996**, *124*, (10), 2322–2339.

Lin, Y.-L.; Farley,R.;Orville,H. Bulk parameterization of the snow field in a cloud model. *J. Climate Appl. Meteor*. **1983,** (22), 1065-1092.

Mei, X.; Bao, J.-W.; Warner, T. T.; Stensrud, D. J. Effect of Time Step in MM5 Simulations of a Mesoscale Convective System. *Mon. Wea. Rev.* **2001**, *129*, (3), 502–516.

Model Evaluation Tools | DTC User's Support Page. http://www.dtcenter.org/met/users/support/ (accessed October 26, 2009).

Skamarock, W. C.; Klemp, J. B.; Dudhia, J.; Gill, D. O.; Barker, D. M.; Duda, M. G.; Huang, X.-Y.; Wang, W.; Powers, J. G. A description of the Advanced Research WRF Version 3; NCAR/TN-475=STR; Mesoscale and Microscale Meteorology Division, National Center of Atmospheric Research: Boulder, CO, June 2008, p. 113.

Thompson, G.; Hall, B.; Field, P.;Rasmussen, R. *A New Bulk Microphysical Parameterization in WRF. 7th WRF Users' Workshop*, Boulder, CO, June 2006.

Wang, Y.; Long, C.N.; Leung,L.R.; Dudhia,J.; McFarlane, S.A.;Mather, J.H.; Ghan, S.J.; Liu,x.; 2009. "Evaluating regional cloud-permitting simulations of the WRF model for the Tropical Warm Pool International Cloud Experiment (TWP-ICE, Darwin, 2006)." Journal of Geophysical Research-Atmosphere, 114, in press.

Wang, W., X. Liu, S. Xie, J. Boyle, and S. McFarlane, 2009: Testing ice microphysics parameterizations in NCAR CAM3 using TWP-ICE data. *J. Geophys. Res.* (in press).

WRF Users Guide. Users Guide for the Advanced Research WRF (ARW) Modeling System Version 3.0; Contents Page. http://www.mmm.ucar.edu/wrf/users/docs/user_guide_V3/contents.html (accessed November 2, 2009).

List of Symbols, Abbreviations, and Acronyms

AFWA	United States Air Force Weather Agency
ARL	U.S. Army Research Laboratory
BED	Battlefield Environment Directorate
CNT	count
DPG	Dugway Proving Ground
etap	eta-pressure
FDDA	four-dimensional data assimilation
h	hour
m/s or m/sec	meters per second
MADIS	Meteorological Assimilation Data Ingest System
MAE	mean absolute error
ME	mean error
MET	Model Evaluation Tool
MYJ	Mellow-Yamada-Janic
NAM	North American Model
NCAR	National Center for Atmospheric Research
NWP	Numerical Weather Prediction
PBL	Planetary boundary layer
PrepBUFR	PrepBinary Universal Form for the Representation
RH	relative humidity
RMSE	root mean square error
RRTM	Rapid Radiative Transfer Model
sec or s	second
SLC	Salt Lake City

TKE	Turbulent Kinetic Energy
UTC	universal time coordinates
WPPV3	Post Processor Version 3
WPPV3	WRF Post Processor Version 3
WRF	Weather Research and Forecasting model
WRF-ARW	Advanced Research version of the Weather Research and Forecasting model
YSU	Yonsei State University

No. of Copies	Organization
1 PDF	ADMNSTR DEFNS TECHL INFO CTR DTIC OCP 8725 JOHN J KINGMAN RD STE 0944 FT BELVOIR VA 22060-6218
3 HCs	US ARMY RSRCH LAB ATTN RDRL CIM P TECHL PUB ATTN RDRL CIM L TECHL LIB ATTN IMNE ALC HRR MAIL & RECORDS MGMT 2800 POWDER MILL ROAD ADELPHI MD 20783-1197
1 CD	US ARMY RSRCH LAB ATTN RDRL CIM G TECHL LIB APG MD 21005-5066
1 CD	NCAR LIBRARY SERIALS NATL CTR FOR ATMOS RSCH PO BOX 3000 BOULDER CO 80307-3000
1 CD	HEADQUARTERS DEPT OF ARMY DAMI-POB WEATHER TEAM 1000 ARMY PENTAGON ROOM 2E383 WASHINGTON DC 20310-1067
1 CD	HQ AFWA DNX 106 PEACEKEEPER DR STE 2N3 OFFUTT AFB NE 68113-4039
1 CD	MAJOR ROBERT A STENGER CHIEF APPLIED OPERATIONS 2D WEATHER GROUP 2 WXG WEA AIR FORCE WEATHER AGENCY 101 NELSON DR OFFUTT AFB NE 68113-4039
1 CD	MR STEVEN A RUGG CHIEF FINE SCALE MODELS TEAM ENVIRONMENTAL MODELS BRANCH 2D WEATHER GROUP 2 WXG WE HQ AF WEATHER AGENCY 101 NELSON DRIVE OFFUTT AFB NE 68113-4039
1 CD	MR DANIEL ROZEMA AFWA A8P HQ AF WEATHER AGENCY 101 NELSON DRIVE OFFUTT AFB NE 68113-4039
1 CD	WSMR TECH LIBRARY BR STEWS IM IT WSMR NM 88002
1 CD	US ARMY CECOM INFORMATION & INTELLIGENCE WARFARE DIRECTORATE ATTN AMSEL RD IW IP FORT MONMOUTH NJ 07703-5211
1 CD	NAVAL RESEARCH LABORATORY MARINE METEOROLOGY DIVISION 7 GRACE HOPPER AVENUE STOP 2 MONTEREY CA 93943-5502
3 HCs 4 CDs	US ARMY RESEARCH LAB ATTN RDRL CIE M J PASSNER WSMR NM 88002-5501
1 CD	US ARMY RESEARCH LAB ATTN RDRL CIE M R DUMAIS WSMR NM 88002-5501
1 CD	US ARMY RESEARCH LAB ATTN RDRL CIE M R FLANIGAN WSMR NM 88002-5501
1 CD	US ARMY RESEARCH LAB ATTN RDRL CIE M D KNAPP WSMR NM 88002-5501
Total 24	(1 PDF, 6 HCs, 17 CDs)

INTENTIONALLY LEFT BLANK.